Applied Energy 361 (2024) 122917

Contents lists available at ScienceDirect

Applied Energy

journal homepage: www.elsevier.com/locate/apenergy

# Model predictive control of a dual fluidized bed gasification plant

Lukas Stanger [a,*], Alexander Bartik [b], Martin Hammerschmid [b], Stefan Jankovic [c], Florian Benedikt [b], Stefan Müller [b,c], Alexander Schirrer [a], Stefan Jakubek [a], Martin Kozek [a]

[a] TU Wien, Institute of Mechanics and Mechatronics, Getreidemarkt 9, 1060 Vienna, Austria
[b] TU Wien, Institute of Chemical, Environmental and Bioscience Engineering, Getreidemarkt 9, 1060 Vienna, Austria
[c] Verto Engineering GmbH, Franz-Josefs Kai 53/13, 1010 Vienna, Austria

## GRAPHICAL ABSTRACT

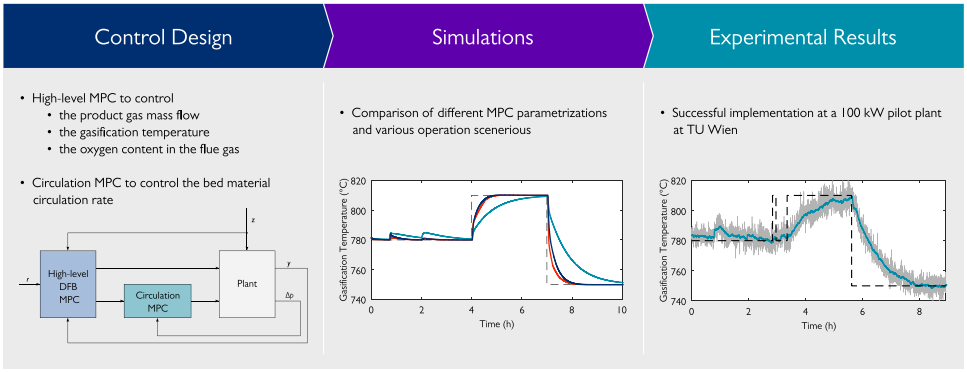


## ARTICLE INFO

*Keywords:*
Model predictive control
Automatic control
DFB
Gasification
Biomass
Fluidized bed

## ABSTRACT

Dual fluidized bed (DFB) gasification is a promising method for producing valuable gaseous energy carriers from biogenic feedstocks as a substitute for fossil fuels. State-of-the-art DFB gasification plants mainly rely on manual operation or single-input single-output control loops, and scientific contributions only exist for controlling individual process variables. This leaves a research gap in terms of comprehensive control strategies for DFB gasification. To address this gap, we propose a multivariate control strategy that focuses on crucial process variables, such as product gas quantity, gasification temperature, and bed material circulation rate. Our approach utilizes model predictive control (MPC), which enables effective process control while explicitly considering process constraints. A simulation study is given demonstrating how different MPC parametrizations influence the behavior of the closed-loop system. Experimental results from a 100 kW pilot plant at TU Wien demonstrate the successful control achieved by the proposed control algorithm.

## 1. Introduction

The need to reduce greenhouse gas emissions calls for substitutes for fossil fuels [1]. Thermo-chemical conversion of biogenic feedstock is promising to generate environmentally friendly energy carriers. Dual fluidized bed (DFB) steam gasification offers a method to produce a product gas containing mainly hydrogen, carbon monoxide, and methane from different biogenic feedstocks [2]. The product gas is almost free of nitrogen and can undergo further processing, such as converting it into synthetic natural gas [3,4], Fischer–Tropsch products [5,6], or pure hydrogen [7,8].

DFB gasification has been successfully implemented on an industrial scale at various locations, including Güssing (AT) [9], Senden

* Corresponding author.
*E-mail address:* lukas.stanger@tuwien.ac.at (L. Stanger).

https://doi.org/10.1016/j.apenergy.2024.122917
Received 15 September 2023; Received in revised form 1 February 2024; Accepted 23 February 2024
Available online 26 February 2024

## Nomenclature

### Abbreviations

| | |
|---|---|
| bm | Biomass |
| CR | Combustion reactor |
| DFB | Dual fluidized bed |
| FG | Flue gas |
| GR | Gasification reactor |
| ILS | Internal loop seal |
| LLS | Lower loop seal |
| MPC | Model predictive control(ler) |
| PG | Product gas |
| ULS | Upper loop seal |

### Mathematical notation and accents

| | |
|---|---|
| $\bar{x}$ | Steady-state target value for $x$ |
| $\boldsymbol{x}^T$ | Transpose of $\boldsymbol{x}$ |
| $\hat{x}$ | Estimate of $x$ |
| $\|\boldsymbol{x}\|$ | Euclidean norm of $\boldsymbol{x}$ |
| diag($\boldsymbol{x}$) | Matrix with the elements of vector $\boldsymbol{x}$ on the main diagonal |
| $x_{k\|j}$ | $j$th element of the vector $\boldsymbol{x}_k$ |
| $x^+$ | One-step-ahead prediction of $x$ |

### Subscripts

| | |
|---|---|
| $i$ | Time step within prediction horizon |
| $k$ | Time step |
| c | Circulation MPC |
| m | Measurement |

### Variables and parameters

| | |
|---|---|
| $\alpha$ | Heat transfer coefficient (kW/°C) |
| $\beta_0, \beta_1$ | Heat transport (bed material) parameters (kW/°C and kW/(mbar °C)) |
| $\boldsymbol{A}$ | System matrix |
| $\boldsymbol{B}$ | Control input matrix |
| $\boldsymbol{B_d}$ | Disturbance state input matrix |
| $\boldsymbol{C}$ | Output matrix |
| $\boldsymbol{C_d}$ | Disturbance state output matrix |
| $\boldsymbol{d}$ | Disturbance state vector |
| $\boldsymbol{E}$ | Disturbance input matrix |
| $\boldsymbol{H}$ | Controlled output matrix |
| $\boldsymbol{h}_{O_2}^T$ | Oxygen content selection vector |
| $\boldsymbol{I}$ | Identity matrix |
| $\boldsymbol{L}$ | Kalman gain matrix |
| $\boldsymbol{Q}$ | State deviation weighting matrix |
| $\boldsymbol{R}$ | Input deviation weighting matrix |
| $\boldsymbol{r}$ | Reference vector |
| $\boldsymbol{R}_\Delta$ | Input rate weighting matrix |
| $\boldsymbol{R}_\infty$ | Weighting matrix for steady-state control inputs |
| $\boldsymbol{u}$ | Control input vector |
| $\boldsymbol{u}^*$ | Desired input vector |
| $\boldsymbol{v}$ | Output noise |
| $\boldsymbol{w}$ | Process noise |
| $\boldsymbol{x}$ | State vector |
| $\boldsymbol{y}$ | Output vector |
| $\boldsymbol{y}^*$ | Controlled output vector |
| $\boldsymbol{z}$ | Disturbance input vector |
| $\Delta p$ | Pressure difference in the upper part of the combustion reactor (mbar) |
| $\Delta t_f$ | Sampling time for fast sampled model (s) |
| $\Delta t_s$ | Sampling time for slowly sampled model (s) |
| $\dot{H}$ | Enthalpy flow rate (kW) |
| $\dot{m}$ | Mass flow rate (kg/h) |
| $\dot{Q}$ | Heat flow rate (kW) |
| $\dot{V}$ | Volumetric flow rate ($Nm^3/h$) |
| $\eta$ | Slack variable |
| $\tau$ | Time constant (s) |
| $\varphi_{SF}$ | Steam-to-fuel ratio |
| $b_{0-4}$ | Circulation model parameters |
| $C$ | Heat capacity (kJ/°C) |
| $c_{LS}$ | Loop seal split factor |
| $N_c$ | Length of control horizon |
| $N_p$ | Total length of prediction horizon |
| $N_{p,f}$ | Length of fast sampled prediction horizon |
| $N_{p,s}$ | Length of slowly sampled prediction horizon |
| $T$ | Temperature (°C) |
| $t$ | Time (s) |
| $u$ | Gas velocity (m/s) |
| $u_{mf}$ | Superficial gas velocity for minimum fluidization (m/s) |
| $u_{se}$ | Superficial gas velocity for fast fluidization (m/s) |
| $w_\eta$ | Slack variable weight |
| $w_{ash}$ | Ash content in biomass (weight fraction) |
| $w_{H_2O}$ | Water content in biomass (weight fraction) |
| $y_{O_2}$ | Oxygen concentration in the dry flue gas (Vol.-%) |

(DE) [10], and Gothenburg (SE) [11]. Numerous studies deal with process modeling [2] or the evaluation of process efficiency [12]. Nevertheless, there is a gap in the literature regarding automatic control strategies for DFB gasifiers. Typically, DFB gasification plants are operated manually or employ multiple single-input single-output controllers to regulate important process variables such as product gas quantity, gasification temperature, and oxygen content in the flue gas, as suggested in [13].

In [14], a PID control strategy is presented, which effectively controls the product gas quantity and leads to reduced fuel consumption. Additionally, in [15], a model-based control concept for controlling the circulation of bed material between the gasification reactor (GR) and the combustion reactor (CR) is introduced.

Currently, no multivariate control strategies can be found in literature for DFB gasification plants, capable of simultaneously controlling all relevant process variables. However, implementing such control concepts presents the possibility to enhance process efficiency and reducing operational costs, while combined single-input single-output control loops can lead to unexpected results and even instability in multivariable coupled systems [16].

Model predictive control (MPC) has proven to be highly effective in various process control applications [17]. It has been shown to be efficient in handling multivariate control problems and is able to explicitly account for constraints in the process variables.

In this study, we introduce an MPC strategy for effectively controlling the product gas quantity and the gasification temperature.

Additionally, the controller takes into consideration a predetermined lower limit for the oxygen content in the flue gas, as set by the plant operator. The control problem explicitly incorporates constraints on various variables, including minimum and maximum values for plant feeds, as well as the essential fluidization requirements of the reactors. Our proposed dual-stage control strategy comprises a high-level DFB MPC, responsible for controlling the product gas quantity and the gasification temperature, along with an underlying MPC controlling the bed material circulation.

The remainder of this paper is organized as follows: In Section 2, we provide a concise overview on the process, highlighting its key characteristics relevant for automatic control. In Section 3, we present the model that the MPC utilizes for its predictions. Subsequently, we introduce the control algorithm employed in this study in Section 4. In Section 5, we present a simulation study comparing different controller parametrization as well as experimental results obtained from implementing the controller at a 100 kW pilot plant located at TU Wien.

## 2. Process description

In this section, we want to give a brief description of DFB gasification. More detailed process descriptions are given in [2,18].

In DFB gasification, the process of generating a product gas from biomass is divided into gasification, which takes place in the GR, and combustion in the CR. Bed material constantly circulates between these two reactors and transports ungasified char from the GR to the CR and heat from the CR to the GR. This heat is essential for the overall endothermic steam gasification reactions. Air is fed to the CR only, meaning that the product gas leaving the GR is almost free of nitrogen which would dilute the product gas and reduce its quality.

### 2.1. 100 kW advanced DFB steam gasification pilot plant at TU Wien

Fig. 1 illustrates the design of the advanced DFB gasification pilot plant at TU Wien. The lower GR utilizes steam for fluidization and is operated as a bubbling fluidized bed reactor. A counter-column is positioned above the bubbling bed that contains constrictions in its cross-sectional area. These constrictions enhance the gas-solid contact and residence time of the bed material, thereby aiding in the reduction of tar content [19]. The CR is fluidized by air and is operated as a fast fluidized bed reactor. The two reactors are connected by a lower loop seal (LLS) at the bottom and an upper loop seal (ULS) at the top. The internal loop seal (ILS) is necessary for the internal bed material circulation of the GR. All loop seals are fluidized with steam.

The biomass is fed to the fluidized bed of the GR, where drying, devolatilization, and gasification take place. A part of the biomass remains ungasified and is transported via the LLS to the CR. There, the char is combusted, thereby heating up the bed material. Heating oil is used as an auxiliary fuel in the CR, which is required to compensate for the relatively high heat loss of the pilot plant. The air necessary for combustion is fed into the reactor in three stages. These air flows are referred to as primary air (air 1), secondary air (air 2), and tertiary air (air 3), whereby the primary air is the lowest airflow and the secondary and tertiary air are above it. A larger volume flow of air at a lower entry point leads to increased circulation of the bed material and vice versa. Thus, this air staging can be used to control the mass flow of bed material circulating between the two reactors. The mass flow of circulating bed material cannot be measured directly. However, the pressure difference $\Delta p$ in the upper part of the CR is a reliable indicator of bed material circulation [20]. Therefore, it is subsequently used for bed material circulation control.

Fig. 2 depicts the TU Wien pilot plant. More comprehensive descriptions of this plant are given in [21,22].

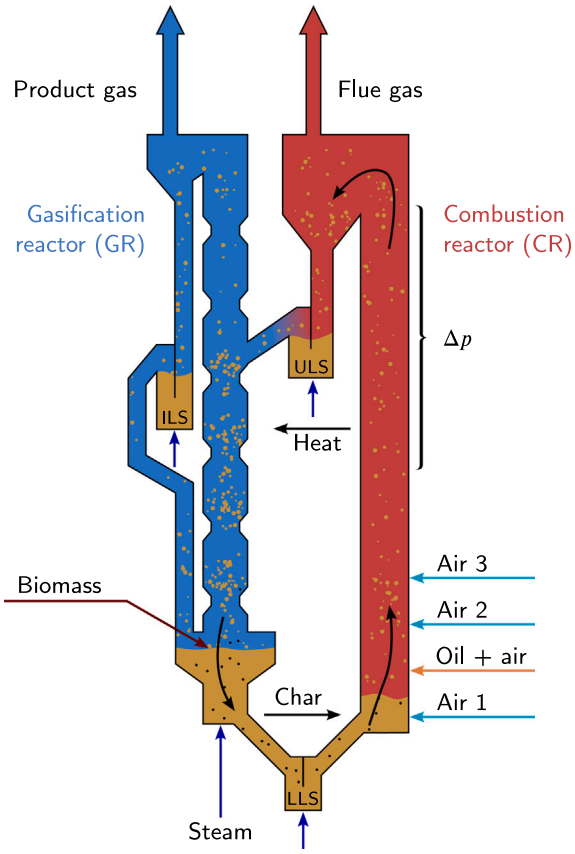


**Fig. 1.** DFB gasification pilot plant at TU Wien (100 kW), with the gasification reactor (GR) at the left and the combustion reactor (CR) at the right.
*Source:* Adapted from [23].

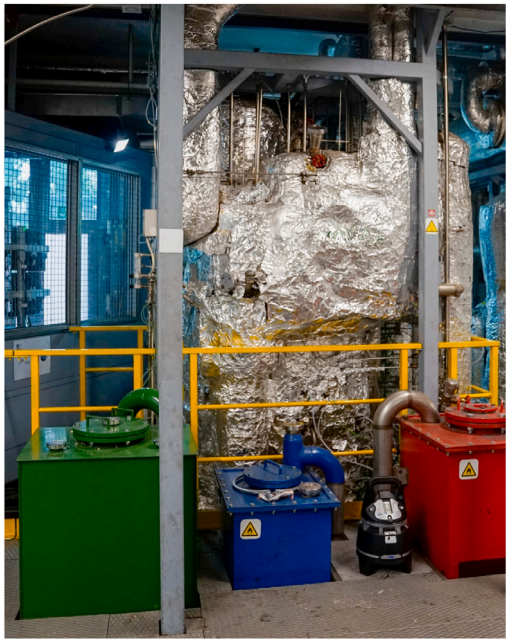

**Fig. 2.** Upper part of the advanced 100 kW pilot plant at TU Wien.

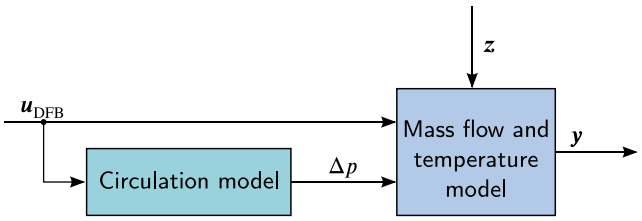


$$\boldsymbol{u}_{\mathrm{DFB}} = \left[\dot{m}_{\mathrm{bm}}, \dot{m}_{\mathrm{oil}}, \dot{m}_{\mathrm{steam,GR}}, \dot{V}_{\mathrm{air1}}, \dot{V}_{\mathrm{air2}}, \dot{V}_{\mathrm{air3}}\right]^T$$
$$\boldsymbol{y} = \left[\dot{m}_{\mathrm{PG}}, \dot{m}_{\mathrm{FG}}, T_{\mathrm{GR}}, T_{\mathrm{CR}}, y_{\mathrm{O_2,FG}}\right]^T$$
$$\boldsymbol{z} = \left[\dot{m}_{\mathrm{steam,ILS}}, \dot{m}_{\mathrm{steam,ULS}}, \dot{m}_{\mathrm{steam,LLS}}, T_{\mathrm{steam}}, T_{\mathrm{air}}\right]^T$$

**Fig. 3.** Structure of the DFB process model, consisting of a gray box model for the mass flows and reactor temperatures and a linear model for the bed material circulation.

## 3. Modeling

The MPC requires a dynamic model that can predict future states and outputs based on system inputs. This model enables the MPC to optimize the future manipulated variables, allowing the process to behave optimally according to predefined objectives.

The majority of dynamic models of DFB gasification rely on computational fluid dynamics, such as the ones presented in [24,25]. These models require a high computational effort and are thus not suitable for MPC. In this work, we are using a model based on the work presented in [23]. This model is based on non-steady-state mass and energy balances.

Maintaining a consistent level of product gas quantity is crucial for subsequent synthesis processes. Thus, it is desirable to control it at a specific value. The gasification temperature has a significant impact on the composition of the product gas [18]. Therefore, it is essential to control these process variables accordingly. The flue gas mass flow and the temperature in the CR are coupled to the product gas mass flow and the gasification temperature, respectively. Thus, these variables are considered in the model as well. In order to achieve complete combustion in the CR, it is desirable to maintain a specific oxygen content in the flue gas. The oxygen content is therefore considered in the model so that it can later be taken into account by the MPC. Thus,

- the product gas mass flow $\dot{m}_{\mathrm{PG}}$,
- the flue gas mass flow $\dot{m}_{\mathrm{FG}}$,
- the temperature in the bubbling bed of the GR $T_{\mathrm{GR}}$, hereinafter referred to as gasification temperature,
- the temperature at the top of the CR $T_{\mathrm{CR}}$, and
- the oxygen content in the dry flue gas $y_{\mathrm{O_2}}$

are modeled, which is summarized in this section. Since the bed material circulation is crucial for the process, a submodel is used to model the pressure difference $\Delta p$ in the upper part of the CR. This variable is then used as an input to the energy balance as the bed material circulation determines how much heat is transported from the CR to the GR. Fig. 3 shows the model structure of the dynamic DFB plant model.

### 3.1. Mass balance

A first-order differential equation is used to model the mass flow of product gas $\dot{m}_{\mathrm{PG}}$ leaving the gasification reactor:

$$\frac{\mathrm{d}\dot{m}_{\mathrm{PG}}}{\mathrm{d}t} = \frac{1}{\tau_{\mathrm{PG}}}\left(-\dot{m}_{\mathrm{PG}} + \dot{m}_{\mathrm{bm}}(1-w_{\mathrm{ash}}) + \dot{m}_{\mathrm{steam,GR,total}} - \dot{m}_{\mathrm{char}}\right), \tag{1}$$

with the time constant $\tau_{\mathrm{PG}}$, the mass of biomass fed to the GR $\dot{m}_{\mathrm{bm}}$, the ash content in the biomass $w_{\mathrm{ash}} \in [0,1]$, the total amount of steam entering the GR $\dot{m}_{\mathrm{steam,GR,total}}$, and the char that is transported to the CR via the LLS $\dot{m}_{\mathrm{char}}$. Thus, it is assumed that at steady state, the product gas mass flow is equal to the mass of ash-free biomass, plus the total amount of steam fed to the GR, reduced by the mass of char leaving the GR. Eq. (1) can be interpreted as this static relationship followed by a first-order linear dynamic model. For the char, it is assumed that a constant fraction of the biomass remains ungasified and is transported to the CR. The total amount of steam entering the GR $\dot{m}_{\mathrm{steam,GR,total}}$ is computed as

$$\dot{m}_{\mathrm{steam,GR,total}} = \dot{m}_{\mathrm{steam,GR}} + \dot{m}_{\mathrm{steam,ILS}} + c_{\mathrm{LS}}(\dot{m}_{\mathrm{steam,ULS}} + \dot{m}_{\mathrm{steam,LLS}}), \tag{2}$$

where $\dot{m}_{\mathrm{steam,GR}}$ is the mass flow of steam fed to the bubbling bed of the GR, and $\dot{m}_{\mathrm{steam,ILS}}$, $\dot{m}_{\mathrm{steam,ULS}}$, and $\dot{m}_{\mathrm{steam,LLS}}$ are the mass flows of steam used to fluidize the ILS, the ULS, and the LLS, respectively. The split factor $c_{\mathrm{LS}}$ defines what fraction of steam used to fluidize the ULS and the LLS enters the GR and is assumed to be constant.

Likewise, the mass flow of flue gas $\dot{m}_{\mathrm{FG}}$ is modeled by a first-order differential equation, with

$$\frac{\mathrm{d}\dot{m}_{\mathrm{FG}}}{\mathrm{d}t} = \frac{1}{\tau_{\mathrm{FG}}}(-\dot{m}_{\mathrm{FG}} + \dot{m}_{\mathrm{char}} + \dot{m}_{\mathrm{steam,CR}} + \dot{m}_{\mathrm{air}} + \dot{m}_{\mathrm{oil}}), \tag{3}$$

where $\tau_{\mathrm{FG}}$ is a time constant, $\dot{m}_{\mathrm{steam,CR}}$ is the steam streaming to the CR from the LLS and the ULS, and $\dot{m}_{\mathrm{air}}$ and $\dot{m}_{\mathrm{oil}}$ are the air and oil feed, respectively.

### 3.2. Energy balance

The reactor temperatures are modeled using energy balances for both reactors. The model incorporates two temperature state variables for each reactor. One state variable represents the temperature inside the reactor while the second state variable represents the reactor wall temperature.

For the GR, the energy balance

$$C_{\mathrm{GR}}\frac{\mathrm{d}T_{\mathrm{GR}}}{\mathrm{d}t} = \dot{H}_{\mathrm{bm}} + \dot{H}_{\mathrm{steam,GR,total}} - \dot{H}_{\mathrm{char}} - \dot{H}_{\mathrm{PG}} + \dot{Q}_{\mathrm{bed}} - \dot{Q}_{\mathrm{wall,GR}}, \tag{4}$$

models the gasification temperature $T_{\mathrm{GR}}$, where $C_{\mathrm{GR}}$ is a heat capacity and $\dot{H}_{\mathrm{bm}}$, $\dot{H}_{\mathrm{steam,GR,total}}$, $\dot{H}_{\mathrm{char}}$ and $\dot{H}_{\mathrm{PG}}$ are the flows of conventional enthalpy of the biomass, steam, char, and product gas, respectively. The specific values of conventional enthalpy of biomass and char are calculated based on their lower heating values. The lower heating values are computed using Boie's formula, which considers their compositions obtained from compositional analysis. The conventional enthalpy of the product gas is computed using a pseudo-equilibrium model for its composition. $\dot{Q}_{\mathrm{bed}}$ is the heat transported by the bed material from the CR to the GR. $\dot{Q}_{\mathrm{wall,GR}}$ is the heat flow from the gas inside the reactor to the reactor wall and thus represents the coupling between the reactor inside temperature state variable and the reactor wall temperature state variable. The heat balance for the reactor wall

$$C_{\mathrm{GR,wall}}\frac{\mathrm{d}T_{\mathrm{GR,wall}}}{\mathrm{d}t} = \dot{Q}_{\mathrm{wall,GR}} - \dot{Q}_{\mathrm{loss,GR}}, \tag{5}$$

models the temperature of the reactor wall $T_{\mathrm{GR,wall}}$, with the heat capacity $C_{\mathrm{GR,wall}}$ and the heat loss $\dot{Q}_{\mathrm{loss,GR}}$. The heat flow from the GR to the reactor wall is modeled by the equation

$$\dot{Q}_{\mathrm{wall,GR}} = \alpha_{\mathrm{GR}}(T_{\mathrm{GR}} - T_{\mathrm{GR,wall}}), \tag{6}$$

with the heat transfer coefficient $\alpha_{\mathrm{GR}}$. The heat loss $\dot{Q}_{\mathrm{loss,GR}}$ is modeled to be a linear function of $T_{\mathrm{GR}}$, as suggested in [23]. Likewise, for the CR there is one energy balance

$$C_{\mathrm{CR}}\frac{\mathrm{d}T_{\mathrm{CR}}}{\mathrm{d}t} = \dot{H}_{\mathrm{char}} + \dot{H}_{\mathrm{oil}} + \dot{H}_{\mathrm{air}} + \dot{H}_{\mathrm{steam,CR}} - \dot{H}_{\mathrm{FG}} - \dot{Q}_{\mathrm{bed}} - \dot{Q}_{\mathrm{wall,CR}}, \tag{7}$$

for the temperature at the top of the CR $T_{\mathrm{CR}}$, with the heat capacity $C_{\mathrm{CR}}$, the flows of conventional enthalpy $\dot{H}_{\mathrm{oil}}$, $\dot{H}_{\mathrm{air}}$, $\dot{H}_{\mathrm{steam,CR}}$ and $\dot{H}_{\mathrm{FG}}$ of oil, air from the three stages, steam, and flue gas, respectively. For calculating the conventional enthalpy of the flue gas, the composition

calculated as described in Section 3.3 is used. Again, there is a second energy balance

$$C_{\mathrm{CR,wall}}\frac{\mathrm{d}T_{\mathrm{CR,wall}}}{\mathrm{d}t} = \dot{Q}_{\mathrm{wall,CR}} - \dot{Q}_{\mathrm{loss,CR}}, \tag{8}$$

describing the reactor wall temperature $T_{\mathrm{CR,wall}}$, with the heat capacity $C_{\mathrm{CR,wall}}$ and the coupling term

$$\dot{Q}_{\mathrm{wall,CR}} = \alpha_{\mathrm{CR}}(T_{\mathrm{CR}} - T_{\mathrm{CR,wall}}), \tag{9}$$

where $\alpha_{\mathrm{CR}}$ is a heat transfer coefficient. The heat flow of bed material $\dot{Q}_{\mathrm{bed}}$ couples the temperature state variables $T_{\mathrm{GR}}$ and $T_{\mathrm{CR}}$. The work presented in [23] demonstrated a high linear correlation between the heat transported by the bed material per degree temperature difference $\dot{Q}_{\mathrm{bed}}/(T_{\mathrm{CR}} - T_{\mathrm{GR}})$ and the pressure difference in the CR $\Delta p$. Thus, the model

$$\dot{Q}_{\mathrm{bed}} = (\beta_0 + \beta_1 \Delta p)(T_{\mathrm{CR}} - T_{\mathrm{GR}}), \tag{10}$$

is used in this work as well. The parameters $\beta_0$ and $\beta_1$ are estimated from measurement data. Note that this model may not hold true for low $\Delta p$ values. However, it exhibits high accuracy under conditions typical for plant operation.

### 3.3. Combustion model

In the CR, complete combustion and thus a surplus of oxygen is desired. Therefore, the oxygen content of the dry flue gas $y_{\mathrm{O_2}}$ is modeled, which allows the MPC to predict the oxygen content and ensure that complete combustion is maintained. It is assumed, that there is always enough air $\dot{V}_{\mathrm{air}}$ available, and that complete combustion of the char $\dot{m}_{\mathrm{char}}$ and the oil $\dot{m}_{\mathrm{oil}}$ is possible. Assuming ideal gases, the oxygen content of the dry flue gas can be computed by

$$y_{\mathrm{O_2}} = \frac{\dot{n}_{\mathrm{O_2,FG}}}{\dot{n}_{\mathrm{CO_2,FG}} + \dot{n}_{\mathrm{N_2,FG}} + \dot{n}_{\mathrm{O_2,FG}}}, \tag{11}$$

where $\dot{n}_{\mathrm{O_2,FG}}$, $\dot{n}_{\mathrm{CO_2,FG}}$, and $\dot{n}_{\mathrm{N_2,FG}}$ are the molar flows of $O_2$, $CO_2$, and $N_2$ in the flue gas, respectively. Other minor components are neglected in this work. Using the stoichiometric combustion equation

$$\mathrm{C}_{\xi_1}\mathrm{H}_{\xi_2}\mathrm{O}_{\xi_3}\mathrm{N}_{\xi_4} + (\xi_1 + \frac{\xi_2}{4} - \frac{\xi_3}{2})\mathrm{O_2} \rightarrow \xi_1\mathrm{CO_2} + \frac{\xi_2}{2}\mathrm{H_2O} + \frac{\xi_4}{2}\mathrm{N_2}, \tag{12}$$

the steady-state oxygen content in the flue gas can be calculated as

$$y_{\mathrm{O_2}} = \frac{\dot{n}_{\mathrm{O,in}} - 2\dot{n}_{\mathrm{C,in}} - 0.5\dot{n}_{\mathrm{H,in}}}{\dot{n}_{\mathrm{N,in}} + \dot{n}_{\mathrm{O,in}} - 0.5\dot{n}_{\mathrm{H,in}}}, \tag{13}$$

where $\dot{n}_{\mathrm{O,in}}$, $\dot{n}_{\mathrm{C,in}}$, $\dot{n}_{\mathrm{H,in}}$, and $\dot{n}_{\mathrm{N,in}}$ are the flows of oxygen, carbon, hydrogen, and nitrogen to the CR, that are depending on the flow rates of char, oil, and air as well as on their compositions. Samples of the char were collected to analyze its composition. In [26], the composition of the char was investigated in a simulation study for varying gasification temperatures during DFB gasification. Their results show that there are only small variations in the composition of char within the temperature range typically used in the pilot plant operation. These small variations are neglected in this work and a constant char composition is assumed. The composition of the heating oil and the air is known as well. It can be seen from (13), that the steam feed does not influence the oxygen content. Thus, (13) is a nonlinear function of the mass flows of char, oil, and air:

$$y_{\mathrm{O_2}} = \phi(\dot{m}_{\mathrm{char}}, \dot{m}_{\mathrm{oil}}, \dot{V}_{\mathrm{air}}). \tag{14}$$

Since it is observed that a change in the fuel feed or the air feed does not instantly change the oxygen content in the flue gas, the first-order differential equation

$$\frac{\mathrm{d}y_{\mathrm{O_2}}}{\mathrm{d}t} = \frac{1}{\tau_{\mathrm{O_2}}}\left(-y_{\mathrm{O_2}} + \phi(\dot{m}_{\mathrm{char}}, \dot{m}_{\mathrm{oil}}, \dot{V}_{\mathrm{air}})\right), \tag{15}$$

with the time constant $\tau_{\mathrm{O_2}}$ is used to model $y_{\mathrm{O_2}}$. This type of model is known in the literature as a Hammerstein model, a static nonlinear function followed by a linear dynamic model. As per the complete combustion assumption, $y_{\mathrm{O_2}} \geq 0$ has to hold.

### 3.4. Bed material circulation model

The pressure difference $\Delta p$ in the upper part of the CR is an indicator for the amount of bed material circulating between the CR and the GR and can be measured directly. It is used in (10) to compute the heat transported by the bed material. However, this pressure difference cannot be manipulated directly by a controller. Thus, a model is used describing how the variables that can be manipulated affect $\Delta p$. A linear approach

$$\Delta p = b_0 + b_1\dot{V}_{\mathrm{air1}} + b_2\dot{V}_{\mathrm{air2}} + b_3\dot{V}_{\mathrm{air3}} + b_4\dot{m}_{\mathrm{bm}} \tag{16}$$

is used to model $\Delta p$ at steady state as a function of the biomass feed $\dot{m}_{\mathrm{bm}}$, the primary air flow $\dot{V}_{\mathrm{air1}}$, the secondary air flow $\dot{V}_{\mathrm{air2}}$, and the tertiary air flow $\dot{V}_{\mathrm{air3}}$. The coefficients $b_0$, $b_1$, $b_2$, $b_3$ and $b_4$ are estimated from measurement data. In the identification experiment, the total airflow was always higher than 50 $\mathrm{Nm^3/h}$. The model may be invalid for smaller total air volumes.

An increase in the biomass feed or in the air flows cannot instantly lead to a change in the bed material circulation, due to the inertia of the bed material. Moreover, no oscillations can be observed in the bed material circulation when increasing an input step-wise. Therefore, the simplest modeling approach, a first-order differential equation

$$\frac{\mathrm{d}(\Delta p)}{\mathrm{d}t} = \frac{1}{\tau_{\mathrm{c}}}\left(-\Delta p + b_0 + b_1\dot{V}_{\mathrm{air1}} + b_2\dot{V}_{\mathrm{air2}} + b_3\dot{V}_{\mathrm{air3}} + b_4\dot{m}_{\mathrm{bm}}\right), \tag{17}$$

with the time constant $\tau_{\mathrm{c}}$ is used to model the lumped dynamic behavior of the bed material circulation.

The equations of the DFB process model are also provided as supplementary material, together with the structure of the linearized model.

## 4. Controller design

DFB gasification plants are typically operated at a steady-state operating point and constant references need to be tracked. Around an operating point, the system behavior can be approximated sufficiently by a linear model. Therefore, linear MPC formulations are used.

Offset-free reference tracking can be achieved by using the so-called velocity form model [27], or by using a disturbance model to account for a plant-model mismatch and constant disturbances [28]. In this work, we use disturbance models to achieve offset-free control. This allows the absolute values of the control inputs to be weighted, which is beneficial in this application as there are more control inputs available than outputs to track.

The subsequent sections discuss the control structure, followed by the design of the high-level DFB MPC and the circulation MPC.

### 4.1. Control structure

The controller for the DFB gasification plant is designed in a way that a constant reference for the product gas mass flow and for the gasification temperature can be tracked without stationary error. For the oxygen content in the flue gas, a lower bound can be set that is considered by the controller. The control scheme for the DFB gasification plant is illustrated in Fig. 4. The high-level DFB MPC uses the biomass feed, the oil feed, the steam feed, the total airflow to the CR, and the bed material circulation rate as control inputs. The adjustment of the steam used to fluidize the loop seals relies on manual valves for the pilot plant and can thus not be manipulated by the controller. Therefore, the mass flows of steam fed to the seals, together with the temperatures of both the incoming air and steam supplied to the plant, are considered as measured disturbances. A secondary MPC serves as a circulation controller, ensuring the desired circulation of bed material by appropriately distributing the total airflow among the three air stages. This hierarchical control structure allows for easier adaptation to different plants, as the specific air staging required for circulation control may vary across different plants.

Both MPCs use linearized discrete-time models for state estimation and prediction. These models are augmented by disturbance states as proposed in [28,29]. In operation, the steps

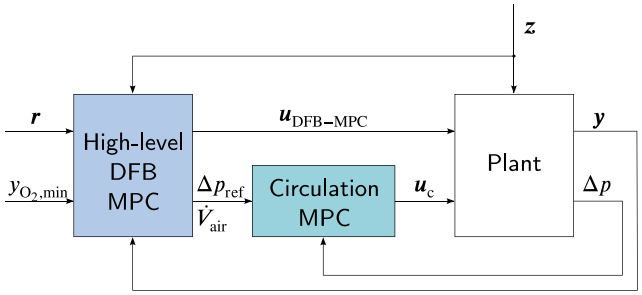


$$\boldsymbol{r} = \left[\dot{m}_{\mathrm{PG,ref}}, T_{\mathrm{GR,ref}}\right]^T$$
$$\boldsymbol{u}_{\mathrm{DFB-MPC}} = \left[\dot{m}_{\mathrm{bm}}, \dot{m}_{\mathrm{oil}}, \dot{m}_{\mathrm{steam,GR}}\right]^T$$
$$\boldsymbol{u}_{\mathrm{c}} = \left[\dot{V}_{\mathrm{air1}}, \dot{V}_{\mathrm{air2}}, \dot{V}_{\mathrm{air3}}\right]^T$$
$$\boldsymbol{y} = \left[\dot{m}_{\mathrm{PG}}, \dot{m}_{\mathrm{FG}}, T_{\mathrm{GR}}, T_{\mathrm{CR}}, y_{\mathrm{O_2}}\right]^T$$
$$\boldsymbol{z} = \left[\dot{m}_{\mathrm{steam,ILS}}, \dot{m}_{\mathrm{steam,ULS}}, \dot{m}_{\mathrm{steam,LLS}}, T_{\mathrm{steam}}, T_{\mathrm{air}}\right]^T$$

**Fig. 4.** Control Structure for DFB gasification plant control.

1. estimation of both the system states and the disturbance states using a Kalman filter,
2. computation of a target input vector and a target state vector, so that the reference is met at steady state, and
3. solving the MPC optimization problem to track the target operating point computed in Step 2,

are repeated at each time step for both the high-level DFB MPC and the circulation MPC.

### 4.2. High-level DFB MPC

The high-level DFB MPC controls the product gas mass flow $\dot{m}_{\mathrm{PG}}$, the gasification temperature $T_{\mathrm{GR}}$, and the oxygen concentration in the flue gas $y_{\mathrm{O_2}}$.

#### 4.2.1. DFB model

The MPC model utilized is a linearized and discretized version derived from the model presented in Section 3. Linearization and discretization leads to the following model:

$$\begin{aligned}\boldsymbol{x}_{k+1} &= \boldsymbol{A}\boldsymbol{x}_k + \boldsymbol{B}\boldsymbol{u}_k + \boldsymbol{E}\boldsymbol{z}_k,\\ \boldsymbol{y}_k &= \boldsymbol{C}\boldsymbol{x}_k,\\ \boldsymbol{y}_k^* &= \boldsymbol{H}\boldsymbol{y}_k,\end{aligned} \tag{18}$$

with the state vector

$$\boldsymbol{x} = \left[\dot{m}_{\mathrm{PG}}, \dot{m}_{\mathrm{FG}}, T_{\mathrm{GR}}, T_{\mathrm{GR,wall}}, T_{\mathrm{CR}}, T_{\mathrm{CR,wall}}, y_{\mathrm{O_2}}\right]^T,$$

the vector of control inputs

$$\boldsymbol{u} = \left[\dot{m}_{\mathrm{bm}}, \dot{m}_{\mathrm{oil}}, \dot{m}_{\mathrm{steam,GR}}, \dot{V}_{\mathrm{air}}, \Delta p\right]^T,$$

the vector of measured disturbances

$$\boldsymbol{z} = \left[\dot{m}_{\mathrm{steam,ILS}}, \dot{m}_{\mathrm{steam,ULS}}, \dot{m}_{\mathrm{steam,LLS}}, T_{\mathrm{steam}}, T_{\mathrm{air}}\right]^T,$$

the output vector

$$\boldsymbol{y} = \left[\dot{m}_{\mathrm{PG}}, \dot{m}_{\mathrm{FG}}, T_{\mathrm{GR}}, T_{\mathrm{CR}}, y_{\mathrm{O_2}}\right]^T,$$

and the vector of controlled outputs

$$\boldsymbol{y}^* = \left[\dot{m}_{\mathrm{PG}}, T_{\mathrm{GR}}\right]^T.$$

The matrices $\boldsymbol{A}$, $\boldsymbol{B}$, $\boldsymbol{C}$ and $\boldsymbol{E}$ are the system matrix, the input matrix, the output matrix, and the disturbance input matrix, respectively. The matrix $\boldsymbol{H}$ selects the controlled outputs from the output vector. The index $k \in \mathbb{N}_0$ indicates the time step.

Disturbance states are introduced to account for plant-model mismatch and constant, unmeasured disturbances and thus ensure offset-free reference tracking at steady state, which leads to the augmented model

$$\begin{aligned}\begin{bmatrix}\boldsymbol{x}_{k+1}\\ \boldsymbol{d}_{k+1}\end{bmatrix} &= \begin{bmatrix}\boldsymbol{A} & \boldsymbol{B}_d\\ \boldsymbol{0} & \boldsymbol{I}\end{bmatrix}\begin{bmatrix}\boldsymbol{x}_k\\ \boldsymbol{d}_k\end{bmatrix} + \begin{bmatrix}\boldsymbol{B}\\ \boldsymbol{0}\end{bmatrix}\boldsymbol{u}_k + \begin{bmatrix}\boldsymbol{E}\\ \boldsymbol{0}\end{bmatrix}\boldsymbol{z}_k + \boldsymbol{w}_k,\\ \boldsymbol{y}_k &= \boldsymbol{C}\boldsymbol{x}_k + \boldsymbol{C}_d\boldsymbol{d}_k + \boldsymbol{v}_k.\end{aligned} \tag{19}$$

The process noise $\boldsymbol{w}$ and the output noise $\boldsymbol{v}$ are assumed to be zero-mean and normally distributed. If the number of disturbance states is equal to the number of measured outputs, offset-free reference tracking can be achieved, if the closed-loop system is stable and no constraints are active at steady state. If the number of disturbance states is chosen to be smaller than the number of measured outputs, then this is not necessarily the case [28]. Thus, we augment the model with 5 disturbance states in this work. The matrix $\boldsymbol{C}_d$ is chosen to be the zero matrix and $\boldsymbol{B}_d$ is designed in a way that the disturbance vector becomes

$$\boldsymbol{d} = \left[\dot{m}_{\mathrm{GR}}, \dot{m}_{\mathrm{CR}}, \dot{Q}_{\mathrm{GR}}, \dot{Q}_{\mathrm{CR}}, y_{\mathrm{O_{2,off}}}\right]^T, \tag{20}$$

where $\dot{m}_{\mathrm{GR}}$ and $\dot{m}_{\mathrm{CR}}$ are unmodeled mass flows to the GR and the CR, $\dot{Q}_{\mathrm{GR}}$ and $\dot{Q}_{\mathrm{CR}}$ are unmodeled heat flows or losses to the two reactors and $y_{\mathrm{O_{2,off}}}$ is the plant-model mismatch for the oxygen concentration in the flue gas. None of these states directly affect the controlled outputs $\boldsymbol{y}_k$ ($\boldsymbol{C}_d = \boldsymbol{0}$). This allows a physical interpretation of the disturbance states. Unmeasured mass flows to the GR $\dot{m}_{\mathrm{GR}}$, for example, can indicate deviations in the measurements of the fuel feed or the product gas mass flow. Biased measurements can particularly arise in the fuel input since the determination of the fuel feed is based on the rotational speed of the dosing screws and their calibrations. Another possible choice for the disturbance state affecting the last output, the oxygen concentration in the flue gas, would be the mass flow of char to the CR. With this choice, the measured oxygen content in the flue gas could be used to monitor the char flow to the CR. However, this would have the consequence that measurement errors, e.g. in the oil feed, would bias the estimate of the char flow. A biased estimate of the char flow would then affect the energy balance of the GR and, thus, the prediction of the gasification temperature. Therefore, we have chosen the last disturbance state to simply be the offset between the modeled oxygen concentration and its measurement.

#### 4.2.2. DFB observer design

A Kalman filter is used to estimate both the system states and the disturbance states by a prediction step

$$\begin{bmatrix}\hat{\boldsymbol{x}}_{k+1}^+\\ \hat{\boldsymbol{d}}_{k+1}^+\end{bmatrix} = \begin{bmatrix}\boldsymbol{A} & \boldsymbol{B}_d\\ \boldsymbol{0} & \boldsymbol{I}\end{bmatrix}\begin{bmatrix}\hat{\boldsymbol{x}}_k\\ \hat{\boldsymbol{d}}_k\end{bmatrix} + \begin{bmatrix}\boldsymbol{B}\\ \boldsymbol{0}\end{bmatrix}\boldsymbol{u}_k + \begin{bmatrix}\boldsymbol{E}\\ \boldsymbol{0}\end{bmatrix}\boldsymbol{z}_k, \tag{21}$$

and a correction step

$$\begin{aligned}\begin{bmatrix}\hat{\boldsymbol{x}}_k\\ \hat{\boldsymbol{d}}_k\end{bmatrix} &= \begin{bmatrix}\hat{\boldsymbol{x}}_k^+\\ \hat{\boldsymbol{d}}_k^+\end{bmatrix} + \begin{bmatrix}\boldsymbol{L}_x\\ \boldsymbol{L}_d\end{bmatrix}(-\boldsymbol{y}_{\mathrm{m}|k} + \boldsymbol{C}\hat{\boldsymbol{x}}_k^+ + \boldsymbol{C}_d\hat{\boldsymbol{d}}_k^+),\\ \hat{\boldsymbol{y}}_k &= \boldsymbol{C}\hat{\boldsymbol{x}}_k + \boldsymbol{C}_d\hat{\boldsymbol{d}}_k,\end{aligned} \tag{22}$$

using the output measurements $\boldsymbol{y}_{\mathrm{m}}$. The steady-state Kalman gain $\boldsymbol{L} = \left[\boldsymbol{L}_{\boldsymbol{x}}^T, \boldsymbol{L}_{\boldsymbol{d}}^T\right]^T$ is computed by solving the discrete-time algebraic Riccati equation [28].

#### 4.2.3. DFB target calculation

A target operating point is determined by a target state $\bar{\boldsymbol{x}}$ and a target control input $\bar{\boldsymbol{u}}$. It is computed so that the vector of tracked outputs $\boldsymbol{y}^*$ meets the reference $\boldsymbol{r}$ at steady state. As there are more control inputs available than output variables that need to be tracked, there is no unique solution for this problem. Given that there is no unique solution for the control input $\bar{\boldsymbol{u}}$ so that the outputs meet the reference, we can specify desired control inputs $\boldsymbol{u}^*$. An optimization problem can be formulated, aiming to make the steady-state input $\bar{\boldsymbol{u}}$ as

close as possible to $\boldsymbol{u}^*$ in a least-squares sense. Using this, additional factors such as economic objectives can be incorporated into the target calculation. We define the optimization problem as follows:

$$\min_{\bar{\boldsymbol{x}}_k, \bar{\boldsymbol{u}}_k} \quad \|\bar{\boldsymbol{u}}_k - \boldsymbol{u}^*\|^2_{\boldsymbol{R}_\infty}, \tag{23a}$$

subject to

$$\begin{bmatrix} \boldsymbol{A} - \boldsymbol{I} & \boldsymbol{B} \\ \boldsymbol{H}\boldsymbol{C} & \boldsymbol{0} \end{bmatrix} \begin{bmatrix} \bar{\boldsymbol{x}}_k \\ \bar{\boldsymbol{u}}_k \end{bmatrix} = \begin{bmatrix} -\boldsymbol{E}\boldsymbol{z}_k - \boldsymbol{B}_d \hat{\boldsymbol{d}}_k \\ \boldsymbol{r}_k - \boldsymbol{H}\boldsymbol{C}_d \hat{\boldsymbol{d}}_k \end{bmatrix}, \tag{23b}$$

$$\boldsymbol{h}^T_{\mathrm{O}_2}(\boldsymbol{C}\bar{\boldsymbol{x}}_k + \boldsymbol{C}_d \hat{\boldsymbol{d}}_k) \geq y_{\mathrm{O}_2,\min}, \tag{23c}$$

$$\varphi_{\mathrm{SF}} = \frac{\bar{u}_{k|3} + \bar{u}_{k|1} w_{\mathrm{H_2O}} + z_{k|1} + c_{\mathrm{LS}}(z_{k|2} + z_{k|3})}{\bar{u}_{k|1}(1 - w_{\mathrm{H_2O}} - w_{\mathrm{ash}})}, \tag{23d}$$

$$\bar{\boldsymbol{u}}_k \in \mathbb{U}, \tag{23e}$$

where $u_{k|j}$ denotes the $j$th element of the vector $\boldsymbol{u}_k$. The matrix $\boldsymbol{R}_\infty$ facilitates the weighting of the individual control inputs' deviation.

The system dynamics is incorporated by the constraint in (23b). The constraint (23c) ensures that the oxygen content in the flue gas is above a predefined limit that can be set by the plant operator. The vector $\boldsymbol{h}^T_{\mathrm{O}_2} = [0, 0, 0, 0, 1]^T$ selects the oxygen concentration in the flue gas from the output vector. With (23d), the steam-to-fuel ratio $\varphi_{\mathrm{SF}}$ can be set to a specific value by the plant operator, where $w_{\mathrm{H_2O}}$ represents the water content in the fuel and $c_{\mathrm{LS}}$ the split factor of both the LLS and the ULS. To further restrict the input space, the constraint (23e) is introduced, which is necessary for two reasons. Firstly, control inputs typically have minimum and maximum values, also due to necessary reactor fluidizations. Secondly, the total airflow to the CR and the bed material circulation rate are interdependent. Consequently, the possible bed material circulation rate heavily relies on the total airflow to the CR. The input constraints are described in detail in Section 4.2.5 and numerical values are given.

The target calculation is performed at every time step $k$ utilizing the current measured disturbance $\boldsymbol{z}$ and the estimate of the disturbance state $\hat{\boldsymbol{d}}$.

Due to the input restrictions, the optimization problem can become infeasible, meaning that no control input can be found so that the reference is reached at steady state. In this case, an alternative optimization problem is solved as suggested in [30]: The distance of the controlled outputs to their reference values is minimized in a least-squares sense instead of (23a). The constraints considered in the alternative optimization problem stay the same as in the original optimization problem (23). This serves as a safety mechanism and was never necessary during the experiment presented in Section 5.

#### 4.2.4. DFB MPC problem

The DFB MPC problem is designed to track the target point computed in Section 4.2.3 by solving the optimization problem

$$\begin{aligned} \min_{\boldsymbol{U}} \quad & \sum_{i=1}^{N_\mathrm{p}} (\|\boldsymbol{x}_{k+i} - \bar{\boldsymbol{x}}_k\|^2_{\boldsymbol{Q}_i} + w_\eta \eta^2_{k+i}) \\ & + \sum_{i=0}^{N_\mathrm{c}-1} (\|\boldsymbol{u}_{k+i} - \bar{\boldsymbol{u}}_k\|^2_{\boldsymbol{R}_i} + \|\Delta \boldsymbol{u}_{k+i}\|^2_{\boldsymbol{R}_\Delta}), \end{aligned} \tag{24a}$$

subject to

$$\boldsymbol{x}_{k+i+1} = \boldsymbol{A}_i \boldsymbol{x}_{k+i} + \boldsymbol{B}_i \boldsymbol{u}_{k+i} + \boldsymbol{E}_i \boldsymbol{z}_k + \boldsymbol{B}_{d|i} \boldsymbol{d}_k, \quad \forall i \in \{0, 1, \dots, N_\mathrm{p} - 1\} \tag{24b}$$

$$\boldsymbol{u}_{k+i} = \boldsymbol{u}_{k+N_\mathrm{c}-1}, \quad \forall i \geq N_\mathrm{c}, \tag{24c}$$

$$\Delta \boldsymbol{u}_{k+i} = \boldsymbol{u}_{k+i} - \boldsymbol{u}_{k+i-1}, \quad \forall i \in \{0, 1, \dots, N_\mathrm{c} - 1\}, \tag{24d}$$

$$\boldsymbol{x}_k = \hat{\boldsymbol{x}}_k, \tag{24e}$$

$$\boldsymbol{d}_k = \hat{\boldsymbol{d}}_k, \tag{24f}$$

$$\boldsymbol{h}^T_{\mathrm{O}_2}(\boldsymbol{C}\bar{\boldsymbol{x}}_k + \boldsymbol{C}_d \hat{\boldsymbol{d}}_k) \geq y_{\mathrm{O}_2,\min} - \eta_{k+i}, \quad \eta_{k+i} \geq 0, \tag{24g}$$

$$\varphi_{\mathrm{SF}} = \frac{u_{k+i|3} + u_{k+i|1} w_{\mathrm{H_2O}} + z_{k|1} + c_{\mathrm{LS}}(z_{k|2} + z_{k|3})}{u_{k+i|1}(1 - w_{\mathrm{H_2O}} - w_{\mathrm{ash}})}, \tag{24h}$$

$$\boldsymbol{u}_{k+i} \in \mathbb{U}. \tag{24i}$$

*Cost function.* The cost function (24a) penalizes a deviation from the target state $\bar{\boldsymbol{x}}_k$ and from the target control input $\bar{\boldsymbol{u}}_k$, weighted by the matrix $\boldsymbol{Q}_i$ and the matrix $\boldsymbol{R}_i$, respectively. The prediction horizon $N_\mathrm{p}$ and the control horizon $N_\mathrm{c}$ are design parameters. Furthermore, changes in the control input are penalized and weighted by $\boldsymbol{R}_\Delta$. To ensure a positive oxygen content in the flue gas, a soft constraint is used, where $\eta$ is a slack variable and $w_\eta$ is the corresponding penalty cost coefficient.

*Constraints.* With (24b) the system dynamics is taken into account. The control horizon can be chosen shorter than the prediction horizon to limit the computational effort. Thus, the control inputs are held constant with (24c) for $i \geq N_\mathrm{c}$. Eqs. (24e) and (24f) consider the initialization of the state predictions with their estimated values. The soft constraint for the oxygen content in the flue gas requires the constraints (24g). The steam-to-fuel ratio is limited to a predefined value as determined by (24h). Finally, the input space is bounded according to the physical limitations of the process by (24i) as specified in Section 4.2.5.

*Non-constant prediction-step MPC.* The time constants of the DFB gasification plant differ strongly. Mass flows and gas compositions change quickly, whereas reactor temperatures change slowly due to the high heat capacities. Therefore, two different models are employed to compute the MPC predictions as proposed in [31]. The first model is created by discretizing the system using a fast sampling time $\Delta t_\mathrm{f}$ and is used to compute the first $N_\mathrm{p,f}$ prediction steps. The second model is obtained by discretization using a slow sampling time $\Delta t_\mathrm{s}$ to compute further $N_\mathrm{p,s}$ predictions. The total number of prediction steps is

$$N_\mathrm{p} = N_\mathrm{p,f} + N_\mathrm{p,s}. \tag{25}$$

The state deviation in (24a) is weighted by the matrix $\boldsymbol{Q}_i$, where

$$\boldsymbol{Q}_i = \begin{cases} \Delta t_\mathrm{f} \boldsymbol{Q} & \forall i \in \{1, \dots, N_\mathrm{p,f}\} \\ \Delta t_\mathrm{s} \boldsymbol{Q} & \forall i \in \{N_\mathrm{p,f} + 1, \dots, N_\mathrm{p}\}. \end{cases} \tag{26}$$

Thus, the integration of the weighted state deviation over time is approximated. The control input deviation is weighted by

$$\boldsymbol{R}_i = \begin{cases} \Delta t_\mathrm{f} \boldsymbol{R} & \forall i \in \{1, \dots, N_\mathrm{p,f}\} \\ \Delta t_\mathrm{s} \boldsymbol{R} & \forall i \in \{N_\mathrm{p,f} + 1, \dots, N_\mathrm{c}\}. \end{cases} \tag{27}$$

It is assumed that $N_\mathrm{p,f} < N_\mathrm{c} < N_\mathrm{p}$.

Riccati terminal costs and suitable terminal constraints around $(\bar{\boldsymbol{x}}_k, \bar{\boldsymbol{u}}_k)$ can be included to ensure closed-loop nominal stability. Extension to robust stability guarantees in the presence of model uncertainties are available in literature [32], but not used in this work.

#### 4.2.5. Input constraints for the high-level DFB MPC

Table 1 presents the implemented minimum and maximum values for the control inputs.

Furthermore, the gas velocities inside the reactors need to satisfy constraints regarding fluidization. For the GR, the boundaries

$$2u_\mathrm{mf} \leq u_\mathrm{GR} \leq u_\mathrm{se} \tag{28}$$

are applied. $u_\mathrm{GR}$ denotes the gas velocity to the GR, depending on the steam feed, the reactor temperature, and the reactor cross-sectional area. The minimum superficial gas velocity $u_\mathrm{mf}$ required for the formation of a bubbling fluidized bed as well as the superficial gas velocity for fast fluidization $u_\mathrm{se}$ depend on gas and bed material properties. For the CR, it is demanded that

$$u_\mathrm{CR} > 0.7 u_\mathrm{se}, \tag{29}$$

**Table 1**
Minimum and maximum values for control inputs (high-level DFB MPC).

| Control input | Min | Max |
|---|---|---|
| $\dot{m}_{\mathrm{bm}}$ | 0 kg/h | 25 kg/h |
| $\dot{m}_{\mathrm{oil}}$ | 0 kg/h | 6.88 kg/h |
| $\dot{m}_{\mathrm{steam,GR}}$ | (28) | 20 kg/h[a] |
| $\dot{V}_{\mathrm{air}}$ | (29) | 100 $\mathrm{Nm^3/h}$ |
| $\Delta p$ | 2 mbar | 10 mbar |

[a] Additionally subject to fluidization constraint (28).

with the gas velocity $u_{\mathrm{CR}}$ in the CR. This has been shown to be an adequate lower limit for the fluidization of the CR. These nonlinear fluidization constraints are linearized at an operating point. Further information on fluidization and the calculation of superficial gas velocities can be found in [33].

Additionally, the total airflow to the CR $\dot{V}_{\mathrm{air}}$ and the pressure difference in the CR $\Delta p$ cannot be chosen independently by the high-level DFB MPC. The pressure difference that can be achieved by varying the air staging depends on the total airflow. These limitations are computed using the circulation model (16).

### 4.3. Circulation MPC

The circulation MPC controls the circulation of bed material between the CR and the GR as demanded by the high-level DFB MPC while ensuring a total volume flow of air to the CR.

#### 4.3.1. Circulation model

For offset-free control of the bed material circulation, the model (17) is augmented by a disturbance state $d_{\mathrm{c}}$, leading to the augmented model

$$\begin{aligned}\dot{x}_{\mathrm{c}} &= \frac{1}{\tau_{\mathrm{c}}}\left(-x_{\mathrm{c}} + b_0 + \begin{bmatrix} b_1 & b_2 & b_3 \end{bmatrix} \boldsymbol{u}_{\mathrm{c}} + b_4 z_{\mathrm{c}} + d_{\mathrm{c}}\right),\\ \dot{d}_{\mathrm{c}} &= 0,\\ y_{\mathrm{c}} &= x_{\mathrm{c}},\end{aligned} \tag{30}$$

with

$$y_{\mathrm{c}} = \Delta p,\ \boldsymbol{u}_{\mathrm{c}} = \begin{bmatrix}\dot{V}_{\mathrm{air1}}, \dot{V}_{\mathrm{air2}}, \dot{V}_{\mathrm{air3}}\end{bmatrix}^T,\ z_{\mathrm{c}} = \dot{m}_{\mathrm{bm}}. \tag{31}$$

#### 4.3.2. Circulation observer design

A Kalman filter is designed for the discrete-time model

$$\begin{aligned}\begin{bmatrix} x_{\mathrm{c}|k+1} \\ d_{\mathrm{c}|k+1} \end{bmatrix} &= \begin{bmatrix} a_{\mathrm{c}} & b_{\mathrm{c}|d} \\ 0 & 1 \end{bmatrix} \begin{bmatrix} x_{\mathrm{c}|k} \\ d_{\mathrm{c}|k} \end{bmatrix} + \begin{bmatrix} \boldsymbol{b}_{\mathrm{c}} \\ \boldsymbol{0} \end{bmatrix} \boldsymbol{u}_{\mathrm{c}|k} + \begin{bmatrix} e_{\mathrm{c}} \\ 0 \end{bmatrix} z_{\mathrm{c}|k} + \boldsymbol{w}_{\mathrm{c}|k},\\ y_{\mathrm{c}|k} &= x_{\mathrm{c}|k} + v_{\mathrm{c}|k},\end{aligned} \tag{32}$$

where $a_{\mathrm{c}}$, $b_{\mathrm{c}|d}$, $\boldsymbol{b}_{\mathrm{c}}$, and $e_{\mathrm{c}}$ are a function of the continuous-time parameters in (30) as well as the sampling time. The estimates for both the system state and the disturbance state are computed by a prediction step

$$\begin{bmatrix} \hat{x}^+_{\mathrm{c}|k+1} \\ \hat{d}^+_{\mathrm{c}|k+1} \end{bmatrix} = \begin{bmatrix} a_{\mathrm{c}} & b_{\mathrm{c}|d} \\ 0 & 1 \end{bmatrix} \begin{bmatrix} \hat{x}_{\mathrm{c}|k} \\ \hat{d}_{\mathrm{c}|k} \end{bmatrix} + \begin{bmatrix} \boldsymbol{b}_{\mathrm{c}} \\ \boldsymbol{0} \end{bmatrix} \boldsymbol{u}_{\mathrm{c}|k} + \begin{bmatrix} e_{\mathrm{c}} \\ 0 \end{bmatrix} z_{\mathrm{c}|k} \tag{33}$$

and a correction step

$$\begin{bmatrix} \hat{x}_{\mathrm{c}|k} \\ \hat{d}_{\mathrm{c}|k} \end{bmatrix} = \begin{bmatrix} \hat{x}^+_{\mathrm{c}|k} \\ \hat{d}^+_{\mathrm{c}|k} \end{bmatrix} + \begin{bmatrix} l_{\mathrm{c}|x} \\ l_{\mathrm{c}|d} \end{bmatrix} (-y_{\mathrm{c|m}|k} + \hat{x}^+_{\mathrm{c}|k}), \tag{34}$$

with the output measurement $y_{\mathrm{c|m}|k}$. The steady-state Kalman gain $\boldsymbol{l}_{\mathrm{c}} = \begin{bmatrix} l_{\mathrm{c}|x}, l_{\mathrm{c}|d} \end{bmatrix}^T$ is computed by solving the discrete-time algebraic Riccati equation [28].

**Table 2**
Minimum and maximum values for control inputs (Circulation MPC).

| Control input | Min | Max |
|---|---|---|
| $\dot{V}_{\mathrm{air1}}$ | 0 $\mathrm{Nm^3/h}$ | 40 $\mathrm{Nm^3/h}$ |
| $\dot{V}_{\mathrm{air2}}$ | 0 $\mathrm{Nm^3/h}$ | 40 $\mathrm{Nm^3/h}$ |
| $\dot{V}_{\mathrm{air3}}$ | 0 $\mathrm{Nm^3/h}$ | 20 $\mathrm{Nm^3/h}$ |

#### 4.3.3. Circulation target calculation

Since three control inputs are available to control the circulation of the bed material while simultaneously ensuring a certain total airflow, there is no unique solution for the air staging. An optimization problem is therefore formulated again. This keeps the control input as close as possible to a desired control input $\boldsymbol{u}^*_{\mathrm{c}}$. The calculation of the target point to be tracked by the MPC is done by solving the optimization problem

$$\min_{\bar{\boldsymbol{u}}_{\mathrm{c}|k}} \|\bar{\boldsymbol{u}}_{\mathrm{c}|k} - \boldsymbol{u}^*_{\mathrm{c}}\|^2, \tag{35a}$$

subject to

$$r_{\mathrm{c}|k} = b_0 + \begin{bmatrix} b_1 & b_2 & b_3 \end{bmatrix} \bar{\boldsymbol{u}}_{\mathrm{c}|k} + b_4 z_{\mathrm{c}|k} + \hat{d}_{\mathrm{c}|k}, \tag{35b}$$

$$\bar{u}_{c|1|k} + \bar{u}_{c|2|k} + \bar{u}_{c|3|k} = \dot{V}_{\mathrm{air,CR}|k}, \tag{35c}$$

$$\bar{\boldsymbol{u}}_{c|k} \in \mathbb{U}_{\mathrm{c}}. \tag{35d}$$

The circulation reference value $r_{\mathrm{c}|k}$ and the total amount of air $\dot{V}_{\mathrm{air,CR}|k}$ are the first values of the control input sequence computed by the high-level DFB MPC. The input space is bounded by (35d) as described in Section 4.3.5.

#### 4.3.4. Circulation MPC problem

The MPC tracks the target point by solving the optimization problem

$$\begin{aligned}\min_{U_{\mathrm{c}}} \quad & \sum_{i=1}^{N_{\mathrm{p}}} (x_{\mathrm{c}|k+i} - r_{\mathrm{c}|k})^2 q_{\mathrm{c}}\\ & + \sum_{i=0}^{N_{\mathrm{c}}-1} (\|\boldsymbol{u}_{\mathrm{c}|k+i} - \bar{\boldsymbol{u}}_{\mathrm{c}|k}\|^2_{\boldsymbol{R}_{\mathrm{c}}} + \|\Delta \boldsymbol{u}_{\mathrm{c}|k+i}\|^2_{\boldsymbol{R}_{\mathrm{c}|\Delta}}),\end{aligned} \tag{36a}$$

subject to

$$\begin{aligned}x_{\mathrm{c}|k+i+1} = a_{\mathrm{c}} x_{\mathrm{c}|k+i} + \boldsymbol{b}_{\mathrm{c}} \boldsymbol{u}_{\mathrm{c}|k+i} + e_{\mathrm{c}} z_{\mathrm{c}|k} + b_{\mathrm{c}|d} d_{\mathrm{c}|k},\\ \forall i \in \{0, 1, \dots, N_{\mathrm{p}} - 1\}\end{aligned} \tag{36b}$$

$$\boldsymbol{u}_{\mathrm{c}|k+i} = \boldsymbol{u}_{\mathrm{c}|k+N_{\mathrm{c}}-1}, \quad \forall i \geq N_{\mathrm{c}}, \tag{36c}$$

$$\Delta \boldsymbol{u}_{\mathrm{c}|k+i} = \boldsymbol{u}_{\mathrm{c}|k+i} - \boldsymbol{u}_{\mathrm{c}|k+i-1}, \quad \forall i \in \{0, 1, \dots, N_{\mathrm{c}} - 1\}, \tag{36d}$$

$$x_{\mathrm{c}|k} = \hat{x}_{\mathrm{c}|k}, \tag{36e}$$

$$d_{\mathrm{c}|k} = \hat{d}_{\mathrm{c}|k}, \tag{36f}$$

$$u_{\mathrm{c}|1|k+i} + u_{\mathrm{c}|2|k+i} + u_{\mathrm{c}|3|k+i} \geq \dot{V}_{\mathrm{air,CR}|k}, \tag{36g}$$

$$\boldsymbol{u}_{\mathrm{c}|k+i} \in \mathbb{U}_{\mathrm{c}}, \tag{36h}$$

where $q_{\mathrm{c}}$ is the weighting for the state deviation, $\boldsymbol{R}_{\mathrm{c}}$ the weighting for the input deviation, and $\boldsymbol{R}_{\mathrm{c}|\Delta}$ the weighting for changes in the control input. To ensure complete combustion, the sum of the three air streams must always be higher than the total amount of air demanded from the high-level DFB MPC. This is taken into account by (36g). Again, the input space is bounded by (36h) according to the input constraints presented in 4.3.5.

#### 4.3.5. Input constraints for the circulation MPC

The minimum and maximum values for the control inputs of the circulation MPC are given in Table 2.

## 5. Results and discussion

The results are presented for the 100 kW pilot plant at TU Wien described in Section 2.1. Before the MPC was implemented, the system was operated manually.

**Table 3**
Prediction and control horizons of the different high-level DFB MPCs.

| | $N_{p,f}$ | $N_{p,s}$ | $\Delta t_f$ | $\Delta t_s$ | $N_c$ |
|---|---|---|---|---|---|
| MPC I | 20 | – | 5 s | – | 20 |
| MPC II | 10 | 30 | 5 s | 250 s | 20 |
| MPC III[a] | 10 | 30 | 5 s | 250 s | 20 |

[a] High weighting of the control input responsible for the bed material circulation rate.

### 5.1. Controller simulation

In order to show the influence of different MPC parametrizations, a simulation study is conducted. Three DFB controllers with different high-level DFB MPC configurations are compared. The three versions differ in their prediction horizons and in their weighting matrices. MPC I utilizes a single time scale for its predictions, resulting in a prediction time of 100 s. MPC II and MPC III utilize the non-constant prediction-step MPC method, which leads to a longer total prediction time of approximately 2 h. Table 3 shows the prediction and control horizons of each MPC. Notably, MPC II and MPC III differ in terms of their weighting matrices. For MPC III, the values in the weighting matrix $\boldsymbol{R}_\infty$ as well as in $\boldsymbol{R}$, penalizing strong deviations from the desired bed material circulation, are chosen very high. This results in constant bed material circulation. The state observer as well as the circulation MPC are the same across all controller configurations. The circulation MPC utilizes a prediction and control horizon of 20 samples. The specific weighting matrices for both the high-level DFB MPCs and the circulation MPC as well as the state observer design matrices are provided in Appendix A. Measurement data from previous test runs were used to determine the covariance matrices for the observer in order to obtain a sufficient result for state estimation. The MPC weighting matrices were tuned in closed-loop simulations.

Two simulations are performed, both starting with reference values for the PG mass flow and the gasification temperature of 30 kg/h and 780 °C, respectively. The minimum value for the $O_2$ concentration in the flue gas is set to 1 Vol.-%, which is appropriate for the pilot plant as the flue gas passes through a post-combustion chamber. For industrial DFB gasification plants, this value may have to be increased. The desired control inputs are set to

$$\boldsymbol{u}^* = \left[20, 4.386, 7.526, 64, 3.5\right]^T \tag{37}$$

for the high-level DFB MPC and to

$$\boldsymbol{u}_c^* = \left[27, 27, 12\right]^T \tag{38}$$

for the circulation MPC. This corresponds to values, where the plant is typically operated and has been operated for identification experiments. The desired steam-to-fuel ratio is set to 0.7.

#### 5.1.1. Tracking of changes in the references

During the first simulation, the following changes in the reference values are applied:

- (a): The reference for the PG mass flow is reduced by 20 %.
- (b): The oil feed in the desired input vector $\boldsymbol{u}^*$ is set from 4.386 kg/h to 0 kg/h. Thus, the oil feed should be reduced by the MPC.
- (c): The reference value for the gasification temperature is increased to 810 °C.
- (d): The reference value for the gasification temperature is decreased to 750 °C.

The simulation results are shown in Fig. 5. The results show the influence of the different MPC parameterizations on the closed-loop dynamics. MPC I focuses on computing steady-state control inputs to achieve desired reference values, resulting in slow dynamics for set-point changes. MPC II uses an extended prediction horizon and higher weighting on deviations of the tracked outputs from their references. This leads to faster closed-loop responses. In the design of MPC III, the bed material circulation is restricted to a specific value. This can be beneficial to ensure a consistent amount of bed material in the counter column of the GR, necessary for gasification reactions. For the simulated plant operation shown in Fig. 5, the following closed-loop behavior can be observed:

- (a): By reducing the product gas mass flow reference, the MPCs reduce biomass and steam inputs. In addition, less heat is required for the endothermic gasification reactions. Therefore, the oil feed is also reduced. The MPC III ensures a constant circulation of the bed material. Since reducing the biomass feed would reduce the bed material circulation, the controller increases air 1 while decreasing air 2 and air 3 to ensure constant circulation. MPC I and MPC II also reduce the bed material circulation due to the lower heat demand.
- (b): MPC I and MPC II are able to reduce the oil feed from a steady-state value of 3.85 kg/h before the change made at $t$ = 2 h to a steady-state value of 3.65 kg/h before $t$ = 4 h, which is a reduction of approximately 5 %. This can be achieved by increasing the bed material circulation. MPC III can hardly reduce the oil consumption, since the bed material circulation has to be held constant.
- (c): MPC I and MPC II achieve the increase in gasification temperature by increasing both the oil feed and the bed material circulation. In addition, the total amount of air must be increased to keep the oxygen content in the flue gas above its lower limit. To increase the bed material circulation, air 1 is increased while air 2 and air 3 are reduced. MPC III achieves the increase in gasification temperature solely by increasing the oil feed, which results in higher oil consumption compared to MPC I and MPC II. The total amount of air to the CR must also be increased, resulting in an increase in all three air streams to keep the circulation rate constant with a higher amount of air. Thus, MPC III increases air 2 and air 3 while MPC I and MPC II decrease them.
- (d): To reduce the gasification temperature, proceed in reverse to the setpoint change (c).

The computation time for each time step, which involves solving the optimization problems for both the high-level DFB MPC and the circulation MPC, is approximately 0.04 s for the configuration with MPC I and approximately 0.07 s for the configuration including MPC II and MPC III.

#### 5.1.2. Simulation with parameter errors in the simulation model

In reality, the plant parameters will differ from the model parameters. In order to investigate the effect of parameter uncertainties, a second simulation is performed. In this simulation, the following parameters are varied in the nonlinear simulation model:

- (e): It is assumed that a constant mass fraction of the dry and ash-free biomass remains ungasified and is transported to the CR as char. This parameter value is increased from 0.05 to 0.065 (+25 %).
- (f): The split factor $c_{LS}$, determining which part of the steam is used to fluidize the ULS and the LLS streams to the GR is increased from 0.5 to 0.7.
- (g): The water content of the biomass is increased from 7.2 % to 20 %.

The results of this simulation are shown in Fig. 6. Here, not all outputs and control inputs are shown, but the most essential ones for investigating these parameter variations. In the following, the closed-loop behavior is discussed for the individual parameter variations:

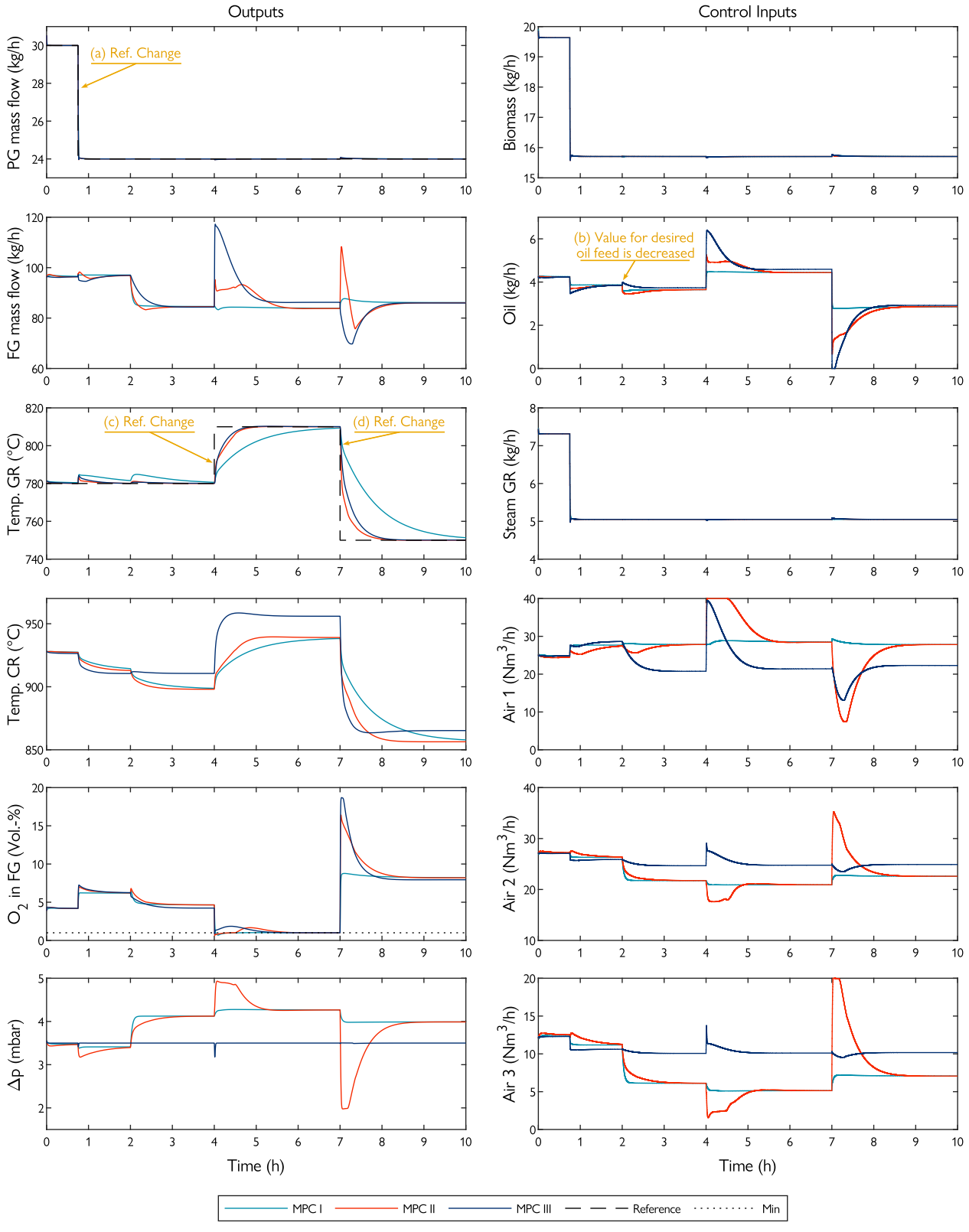


**Fig. 5.** Simulation results comparing three different controllers for the DFB gasification plant. Reference tracking is applied for the PG mass flow and the gasification temperature (Temp. GR) while ensuring a minimum oxygen concentration in the FG. MPC I has been implemented at the TU Wien pilot plant.

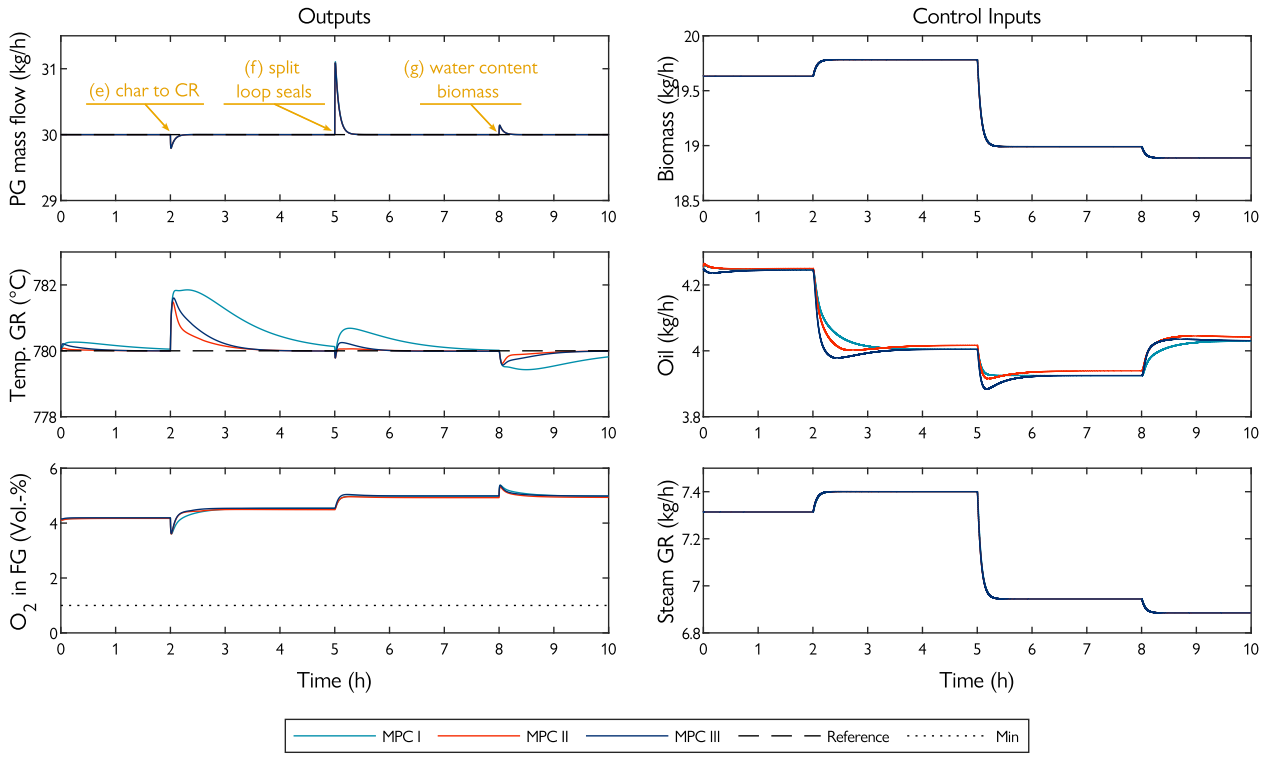


**Fig. 6.** Simulation results to show the influence of parameter deviations between the MPC model and the nonlinear simulation model.

- (e): The controller must increase both the biomass and the steam feed to bring the product gas mass flow back to its reference. More char is combusted in the CR, consequently, the oil feed must be reduced by the controllers.
- (f): The increased amount of steam to the GR results temporarily in a higher product gas mass flow. To compensate, the controller must reduce the feed to the GR. Since the steam-to-fuel ratio is fixed at a certain value, both the biomass and the steam feed are reduced. Due to the reduced biomass feed, less heat is required for the gasification reactions. As a result, the gasification temperature increases, which the controllers compensate for by reducing the oil feed.
- (g): Higher biomass moisture requires more heat to evaporate the water. Thus, the gasification temperature decreases temporarily, which is compensated by an increased oil feed. The model also assumes that a constant fraction of the dry and ash-free biomass is transported to the CR. As the dry and ash-free biomass feed decreases, the char flow to the CR decreases, resulting in a higher product gas mass flow. This is compensated for by the decrease in biomass and steam feed.

The controllers can compensate for the plant model mismatch using the disturbance model, but it takes a while. This is because in the observer design, it is assumed that the disturbances change slowly over time. In this simulation, parameters were changed instantaneously for easier interpretability of the closed-loop results. However, in the real process, parameters will change more slowly, for example, the fraction of biomass transported to the CR may depend on the gasification temperature, which changes slowly over time.

### 5.2. Experimental closed-loop validation on the pilot plant

The implementation and testing of the controller at the pilot plant were conducted in two stages: initially, the circulation MPC was tested independently to ensure its ability to correctly control the bed material circulation. In the second stage, the overall DFB controller, comprising the high-level DFB MPC and the circulation MPC, was tested as a complete system.

**Table 4**
Measurement equipment at the TU Wien pilot plant.
*Source:* Adapted from [23].

| Process variable | Device |
|---|---|
| Temperature | Type K thermocouple |
| Pressure | Kalinsky pressure sensor |
| Steam and air flows | Variable area flowmeter |
| Product gas and flue gas flows | Barthel orifice meter |
| Main gas compositions | Rosemount NGA 2000 |
| Fuel feed | Rot. speed of dosing screws[a] |

[a] The dosing screws are calibrated before every test run.

#### 5.2.1. Experimental setup

For the experimental results presented in this work, softwood pellets were used as feedstock. The bed material inventory initially consisted of 70 kg and was composed of a mixture of 80 % olivine and 20 % limestone.

Table 4 provides an overview of the equipment utilized for measurement purposes. The thermocouples are mounted so that the tip protrudes a few millimeters into the reactor [34]. Detailed information regarding the measurement devices and actuators used at the pilot plant can be found in [35]. The measurement data collected by the plant's process control system is processed at a separate computer running MATLAB every 5 s. Further information regarding the data communication can be found in [36]. The MPC optimization problems are formulated using YALMIP [37] and solved with `quadprog` from the MATLAB optimization toolbox [38].

#### 5.2.2. Circulation MPC tests

Fig. 7 shows the experimental results of the circulation MPC. Reference values were provided for two variables: the bed material circulation, represented by the pressure difference $\Delta p$ in the upper CR, and the total amount of airflow to the CR. These reference values were changed stepwise during the test run. At around $t = 10$ min, for example, the reference for $\Delta p$ is increased while keeping the reference for the

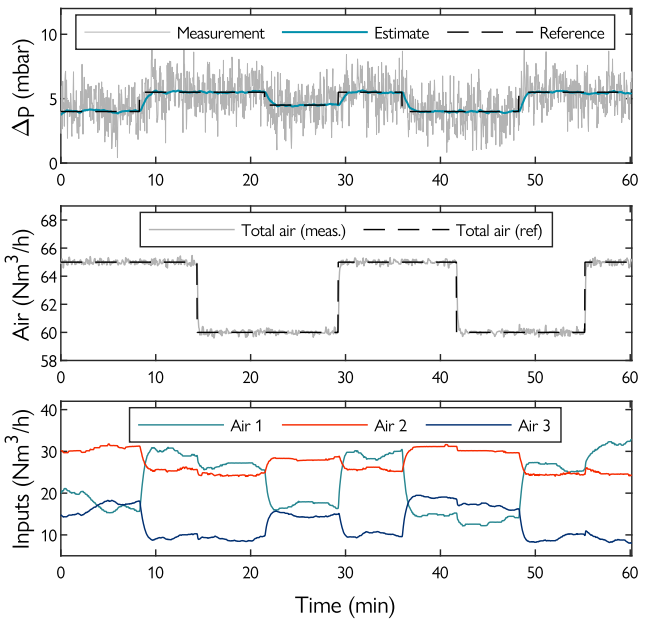


**Fig. 7.** Experimental results from the circulation MPC controlling the bed material circulation at the TU Wien pilot plant.

total airflow constant. The pressure difference can be increased by the circulation controller by increasing air 1 while reducing air 2 and air 3. It can be seen that the bed material circulation reacts quite fast to changes in the air staging.

### 5.2.3. DFB controller tests

The results obtained from the pilot plant controlled by the overall DFB controller, which comprises the high-level DFB MPC (MPC I from Section 5.1) and the circulation MPC, are presented in Fig. 8. Similar to the simulation in Section 5.1.1, the same changes in references were applied. The experimental results show effective control of the DFB gasification pilot plant. The tracking of the reference for the product gas quantity was rapid and efficient. Reference changes for the gasification temperature could be tracked successfully as well. The circulation MPC successfully achieved rapid control of the bed material circulation as required by the high-level DFB MPC, due to the fast dynamics of the circulation. The increase in the reference for the gasification temperature was initially conducted slightly before $t = 3$ h. However, due to the necessity of maintenance of the gas analysis system, the reference value was set back to 780 °C. Manual operation of the plant was required as the maintenance caused wrong measurements in the product gas mass flow. The period during which the plant was operated manually is highlighted in the graph with a gray background. In addition to the raw measurement data, a smoothed signal of the pressure difference $\Delta p$ is shown. The signal has been smoothed by calculating a centered moving average with a window size of 21 samples.

The orifice plates measuring the product gas and flue gas flow rates are flushed every 15 min using nitrogen. This results in peaks in their measurements. Due to the measurement limits of the variable area flowmeter, it was not possible to achieve small flow rates (< 5 $Nm^3/h$ for air 1 and air 2, < 3 $Nm^3/h$ for air 3). This issue affected air 3 between hours 2 and 4. During the test run, there was a calibration error in the dosing screws for the biomass. This resulted in an actual biomass feed that was 20% lower than the values calculated by the MPC. However, this was compensated by the controller by considering the estimated disturbance states. In Fig. 8, the corrected measurements are shown.

Setting the value for the desired oil feed to zero (b), decreased the oil consumption temporarily. However, the oil consumption increased again. A more pronounced impact could be achieved by increasing the corresponding entry in the weighting matrix $\boldsymbol{R}_{\infty}$.

For changes in the reference of the gasification temperature, it took some time for the system to follow the new reference. MPC I was implemented as it is less aggressive than MPC II and MPC III. The simulation results match very well with the experimental results. This shows a high model accuracy. In future experiments, the MPC II or MPC III settings will be tested, which are expected to result in shorter rise times for setpoint changes in the gasification temperature.

## 6. Conclusion and outlook

Within the present work, model predictive control of a DFB gasification plant is investigated. The proposed control concept utilizes two MPCs. Firstly, a high-level DFB MPC is used to control the quantity of PG and the gasification temperature while ensuring a specific minimum oxygen content in the flue gas. Secondly, a circulation MPC controls the circulation of bed material according to the desired settings from the high-level DFB MPC by adjusting the air staging in the CR. This modular control structure is expected to enhance the transferability of the controller to other DFB gasification plants.

In our control strategy, the plant operator specifies the desired values for the gasification temperature and the steam-to-fuel ratio, in addition to other operation targets. These process variables have been identified with respect to their significant influence on the product gas composition. The desired values need to be specified in a way, that the product gas quality meets the expectations of the plant operator regarding product gas quality. The expectations with respect to the product gas quality can differ from case to case depending on the gas utilization pathway as well as local regulations.

The proposed DFB control concept was implemented and successfully tested for over eight hours at the DFB pilot plant in TU Wien. Different setpoints for the PG quantity as well as for the gasification temperature could be tracked successfully. The MPC operates based on physical models, which simplifies the application of the control concept to different fuels and other plants. When applying the controller to different plants, it is necessary to re-estimate the plant-specific model parameters, such as reactor heat capacities or parameters that describe the heat transferred by the bed material.

In industrial-sized plants, PG recirculation is typically employed, and the amount of PG is measured after $H_2O$ separation, while in the considered pilot plant the wet flow of PG was measured and controlled. Controlling the dry quantity of PG that remains after recirculation should be investigated, as the dry PG is the desired product.

Finally, it can be summarized, that the present work was able to demonstrate a control strategy for a DFB gasification plant. Future work will concentrate on the implementation in an operational environment at a larger scale.

## CRediT authorship contribution statement

**Lukas Stanger:** Writing – original draft, Visualization, Validation, Software, Methodology, Conceptualization. **Alexander Bartik:** Writing – review & editing, Resources, Investigation. **Martin Hammerschmid:** Writing – review & editing, Resources, Investigation. **Stefan Jankovic:** Writing – review & editing, Investigation. **Florian Benedikt:** Writing – review & editing, Resources, Investigation. **Stefan Müller:** Writing – review & editing, Resources. **Alexander Schirrer:** Writing – review & editing, Methodology, Conceptualization. **Stefan Jakubek:** Writing – review & editing. **Martin Kozek:** Writing – review & editing, Supervision, Conceptualization.

## Declaration of competing interest

The authors declare that they have no known competing financial interests or personal relationships that could have appeared to influence the work reported in this paper.

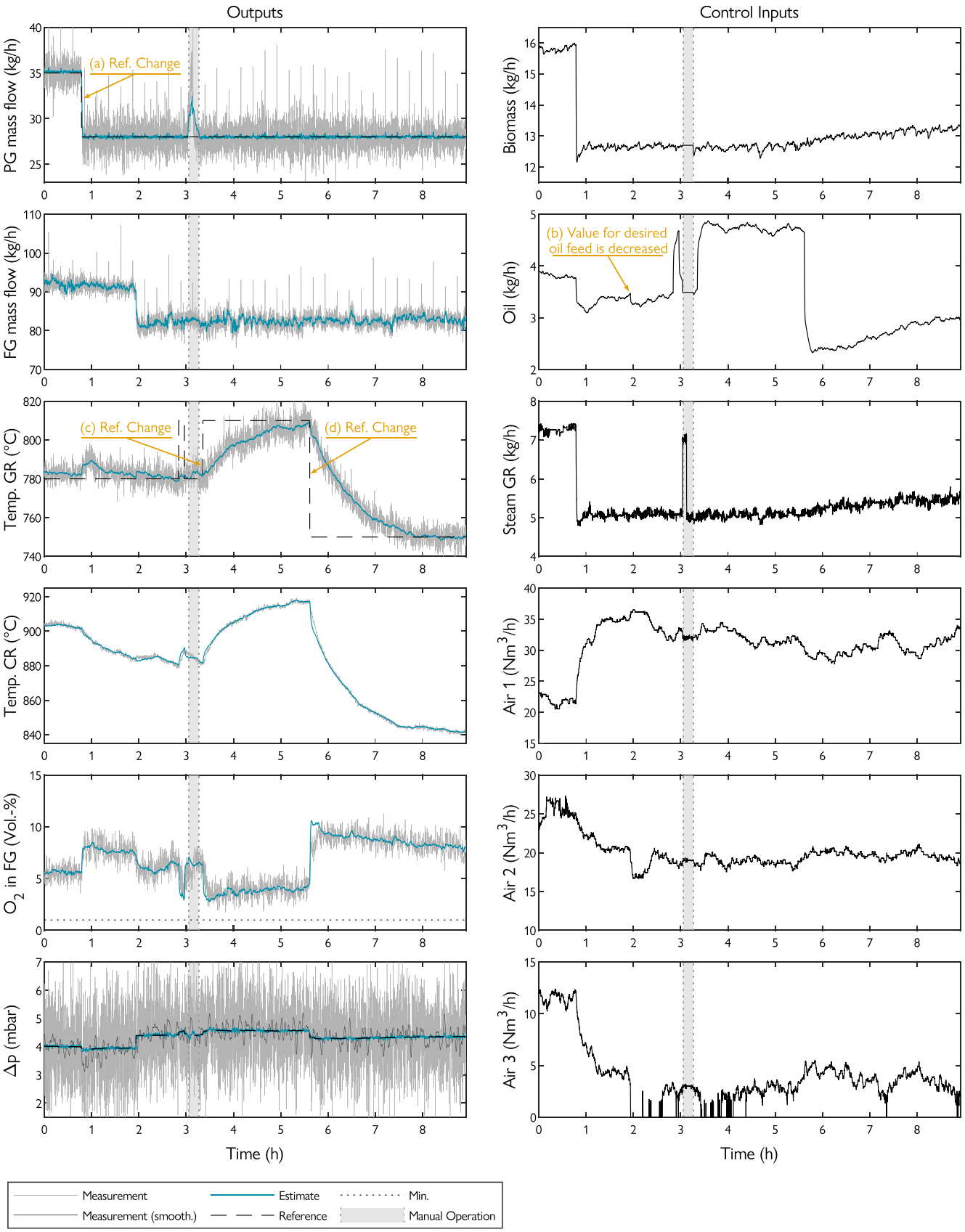


**Fig. 8.** Experimental results from the TU Wien DFB pilot plant controlled by the proposed DFB MPC.

## Data availability

Data will be made available on request.

## Acknowledgments

This work was supported by the project ADORe-SNG, which is funded by the Austrian Climate and Energy Fund (FFG, No. 881135).

The authors acknowledge TU Wien Bibliothek, Austria for financial support through its Open Access Funding Programme.

## Appendix A

### A.1. High-level DFB MPC

All state weighting matrices $\boldsymbol{Q}$ involve a scaling with a state $\boldsymbol{x}_0$

$$\boldsymbol{Q} = \mathrm{diag}(\boldsymbol{x}_0)^{-2}\tilde{\boldsymbol{Q}},$$

where $\tilde{\boldsymbol{Q}}$ is a design matrix that is always diagonal and specified below for the individual MPC configurations. The same applies for the control input weighting matrices

$$\boldsymbol{R} = \mathrm{diag}(\boldsymbol{u}_0)^{-2}\tilde{\boldsymbol{R}},$$
$$\boldsymbol{R}_\Delta = \mathrm{diag}(\boldsymbol{u}_0)^{-2}\tilde{\boldsymbol{R}}_\Delta,$$
$$\boldsymbol{R}_\infty = \mathrm{diag}(\boldsymbol{u}_0)^{-2}\tilde{\boldsymbol{R}}_\infty.$$

The scaling vectors correspond to a state and control input, which represent the typical operating point of the plant and are specified as

$$\boldsymbol{u}_0 = \begin{bmatrix}20, & 4.386, & 7.526, & 64, & 3.5\end{bmatrix}^T,$$
$$\boldsymbol{x}_0 = \begin{bmatrix}29.563, & 96.236, & 782.97, & 736.17, & 932.44, & 925.18, & 3.561\end{bmatrix}^T.$$

The design matrices for the high-level DFB MPC are selected as follows: for *MPC I*,

$$\tilde{\boldsymbol{Q}} = \boldsymbol{I}, \quad w_\eta = 10^8,$$
$$\tilde{\boldsymbol{R}} = \boldsymbol{I}, \quad \tilde{\boldsymbol{R}}_\Delta = 20 \cdot \boldsymbol{I}, \quad \tilde{\boldsymbol{R}}_\infty = \boldsymbol{I},$$

for *MPC II*,

$$\tilde{\boldsymbol{Q}} = \mathrm{diag}(10^4, 1, 10^4, 1, 1, 1, 1), \quad w_\eta = 10^8,$$
$$\tilde{\boldsymbol{R}} = 10 \cdot \boldsymbol{I}, \quad \tilde{\boldsymbol{R}}_\Delta = 10^3 \cdot \boldsymbol{I}, \quad \tilde{\boldsymbol{R}}_\infty = \boldsymbol{I},$$

and for *MPC III*,

$$\tilde{\boldsymbol{Q}} = \mathrm{diag}(10^4, 1, 10^4, 1, 1, 1, 1), \quad w_\eta = 10^8$$
$$\tilde{\boldsymbol{R}} = \mathrm{diag}(10, 10, 10, 10, 10^6), \quad \tilde{\boldsymbol{R}}_\Delta = 10^3 \cdot \boldsymbol{I}$$
$$\tilde{\boldsymbol{R}}_\infty = \mathrm{diag}(1, 1, 1, 1, 10^4)$$

#### A.1.1. Kalman filter design

The steady-state Kalman gain is computed by

$$\boldsymbol{L} = -\boldsymbol{\Sigma}\boldsymbol{C}^T(\boldsymbol{C}\boldsymbol{\Sigma}\boldsymbol{C}^T + \boldsymbol{R}_{\mathrm{KF}})^{-1},$$

where $\boldsymbol{\Sigma}$ is the solution of the discrete-time algebraic Riccati equation

$$\boldsymbol{\Sigma} = \boldsymbol{\mathcal{A}}\boldsymbol{\Sigma}\boldsymbol{\mathcal{A}}^T + \boldsymbol{Q}_{\mathrm{KF}} - \boldsymbol{\mathcal{A}}\boldsymbol{\Sigma}\boldsymbol{C}^T(\boldsymbol{C}\boldsymbol{\Sigma}\boldsymbol{C}^T + \boldsymbol{R}_{\mathrm{KF}})^{-1}\boldsymbol{C}\boldsymbol{\Sigma}\boldsymbol{\mathcal{A}}^T.$$

$\boldsymbol{\mathcal{A}}$ and $\boldsymbol{C}$ denote the system and the output matrix of the augmented system. The process noise covariance matrix $\boldsymbol{Q}_{\mathrm{KF}}$ and the measurement noise covariance matrix $\boldsymbol{R}_{\mathrm{KF}}$ are specified as

$$\boldsymbol{Q}_{\mathrm{KF}} = \mathrm{diag}(10, 10, 10, 10, 10, 10, 10, 1, 1, 1, 1, 1),$$
$$\boldsymbol{R}_{\mathrm{KF}} = 10^3 \cdot \mathrm{diag}(2, 2, 20, 10, 10).$$

### A.2. Circulation MPC

The MPC weighting matrices are defined as

$$q_{\mathrm{c}} = 10^4, \quad \boldsymbol{R}_{\mathrm{c}} = 1.2 \cdot \boldsymbol{I}, \quad \boldsymbol{R}_{\mathrm{c}|\Delta} = 1.2 \cdot 10^3 \cdot \boldsymbol{I}.$$

For the calculation of the steady-state Kalman gain, the covariance matrix of the process noise as well as the covariance of the measurement noise are specified as

$$\boldsymbol{Q}_{\mathrm{c|KF}} = \boldsymbol{I}, \quad r_{\mathrm{c|KF}} = 10^4.$$

## Appendix B. Supplementary data

Supplementary material related to this article can be found online at https://doi.org/10.1016/j.apenergy.2024.122917.

## References

[1] IPCC. Climate Change 2023: Synthesis Report. Geneva, Switzerland: IPCC; 2023.
[2] Hanchate N, Ramani S, Mathpati CS, Dalvi VH. Biomass gasification using dual fluidized bed gasification systems: A review. J Clean Prod 2021;280:123148. http://dx.doi.org/10.1016/J.JCLEPRO.2020.123148.
[3] Bartik A, Benedikt F, Fuchs J, Hofbauer H, Müller S. Experimental investigation of hydrogen-intensified synthetic natural gas production via biomass gasification: a technical comparison of different production pathways. Biomass Convers Biorefinery 2023. http://dx.doi.org/10.1007/s13399-023-04341-3.
[4] Hammerschmid M, Bartik A, Benedikt F, Veress M, Pratschner S, Müller S, et al. Economic and ecological impacts on the integration of biomass-based SNG and FT diesel in the Austrian energy system. Energies 2023;16(16). http://dx.doi.org/10.3390/en16166097.
[5] Chiodini A, Bua L, Carnelli L, Zwart R, Vreugdenhil B, Vocciante M. Enhancements in Biomass-to-Liquid processes: Gasification aiming at high hydrogen/carbon monoxide ratios for direct Fischer-Tropsch synthesis applications. Biomass Bioenergy 2017;106:104–14. http://dx.doi.org/10.1016/J.BIOMBIOE.2017.08.022.
[6] Müller S, Groß P, Rauch R, Zweiler R, Aichernig C, Fuchs M, et al. Production of diesel from biomass and wind power – Energy storage by the use of the Fischer-Tropsch process. Biomass Convers Biorefinery 2018;8(2):275–82. http://dx.doi.org/10.1007/s13399-017-0287-1.
[7] Kraussler M, Binder M, Schindler P, Hofbauer H. Hydrogen production within a polygeneration concept based on dual fluidized bed biomass steam gasification. Biomass Bioenergy 2018;111:320–9. http://dx.doi.org/10.1016/J.BIOMBIOE.2016.12.008.
[8] Loipersböck J, Luisser M, Müller S, Hofbauer H, Rauch R. Experimental demonstration and validation of hydrogen production based on gasification of lignocellulosic feedstock. ChemEngineering 2018;2(4). http://dx.doi.org/10.3390/chemengineering2040061.
[9] Kirnbauer F, Hofbauer H. Investigations on bed material changes in a dual fluidized bed steam gasification plant in güssing, Austria. Energy Fuels 2011;25(8):3793–8. http://dx.doi.org/10.1021/ef200746c.
[10] Kuba M, Kraft S, Kirnbauer F, Maierhans F, Hofbauer H. Influence of controlled handling of solid inorganic materials and design changes on the product gas quality in dual fluid bed gasification of woody biomass. Appl Energy 2018;210:230–40. http://dx.doi.org/10.1016/J.APENERGY.2017.11.028.
[11] Thunman H, Seemann M, Berdugo Vilches T, Maric J, Pallares D, Ström H, et al. Advanced biofuel production via gasification – lessons learned from 200 man-years of research activity with Chalmers' research gasifier and the GoBiGas demonstration plant. Energy Sci Eng 2018;6(1):6–34. http://dx.doi.org/10.1002/ese3.188.
[12] Heyne S, Thunman H, Harvey S. Exergy-based comparison of indirect and direct biomass gasification technologies within the framework of bio-SNG production. Biomass Convers Biorefinery 2013;3(4):337–52. http://dx.doi.org/10.1007/s13399-013-0079-1.
[13] Pröll T, Hofbauer H. Process and device for providing a constant product gas rate from a fluidized bed gas generation plant. 2010, WO2010006353A3.
[14] Nigitz T, Gölles M, Aichernig C, Schneider S, Hofbauer H, Horn M. Increased efficiency of dual fluidized bed plants via a novel control strategy. Biomass Bioenergy 2020;141:105688. http://dx.doi.org/10.1016/J.BIOMBIOE.2020.105688.
[15] Stanger L, Schirrer A, Bartik A, Kozek M. Minimum-variance model predictive control for dual fluidized bed circulation control. IFAC-PapersOnLine 2023;56(2):2701–6. http://dx.doi.org/10.1016/j.ifacol.2023.10.1364.
[16] Glad T, Ljung L. Control theory. CRC Press; 2000, http://dx.doi.org/10.1201/9781315274737.
[17] Schwenzer M, Ay M, Bergs T, Abel D. Review on model predictive control: an engineering perspective. Int J Adv Manuf Technol 2021;117(5):1327–49. http://dx.doi.org/10.1007/s00170-021-07682-3.

[18] Karl J, Pröll T. Steam gasification of biomass in dual fluidized bed gasifiers: A review. Renew Sustain Energy Rev 2018;98:64–78. http://dx.doi.org/10.1016/J.RSER.2018.09.010.
[19] Mauerhofer AM, Schmid JC, Benedikt F, Fuchs J, Müller S, Hofbauer H. Dual fluidized bed steam gasification: Change of product gas quality along the reactor height. Energy 2019;173:1256–72. http://dx.doi.org/10.1016/J.ENERGY.2019.02.025.
[20] Fuchs J, Schmid J, Benedikt F, Mauerhofer A, Muller S, Hofbauer H. A general method for the determination of the entrainment in fluidized beds. Int J Multiphys 2018;12(4):359–72. http://dx.doi.org/10.21152/1750-9548.12.4.359.
[21] Schmid JC, Benedikt F, Fuchs J, Mauerhofer AM, Müller S, Hofbauer H. Syngas for biorefineries from thermochemical gasification of lignocellulosic fuels and residues—5 years' experience with an advanced dual fluidized bed gasifier design. Biomass Convers Biorefinery 2021;11(6):2405–42. http://dx.doi.org/10.1007/s13399-019-00486-2.
[22] Benedikt F. Fuel flexible advanced dual fluidized bed steam gasification [Ph.D. thesis], TU Wien; 2020, http://dx.doi.org/10.34726/hss.2020.39988.
[23] Stanger L, Schirrer A, Benedikt F, Bartik A, Jankovic S, Müller S, et al. Dynamic modeling of dual fluidized bed steam gasification for control design. Energy 2023;265:126378. http://dx.doi.org/10.1016/J.ENERGY.2022.126378.
[24] Sun H, Bao G, Yang S, Hu J, Wang H. Numerical study of the biomass gasification process in an industrial-scale dual fluidized bed gasifier with 8MWth input. Renew Energy 2023;211:681–96. http://dx.doi.org/10.1016/J.RENENE.2023.04.118.
[25] Liu H, Cattolica RJ, Seiser R, Liao Ch. Three-dimensional full-loop simulation of a dual fluidized-bed biomass gasifier. Appl Energy 2015;160:489–501. http://dx.doi.org/10.1016/J.APENERGY.2015.09.065.
[26] Abdelouahed L, Authier O, Mauviel G, Corriou JP, Verdier G, Dufour A. Detailed modeling of biomass gasification in dual fluidized bed reactors under aspen plus. Energy Fuels 2012;26(6):3840–55. http://dx.doi.org/10.1021/ef300411k.
[27] Wang L. A Tutorial on Model Predictive Control: Using a Linear Velocity-Form Model. Dev Chem Eng Miner Process 2004;12(5–6):573–614. http://dx.doi.org/10.1002/apj.5500120511.
[28] Pannocchia G, Rawlings JB. Disturbance models for offset-free model-predictive control. AIChE J 2003;49(2):426–37. http://dx.doi.org/10.1002/aic.690490213.
[29] Maeder U, Borrelli F, Morari M. Linear offset-free model predictive control. Automatica 2009;45(10):2214–22. http://dx.doi.org/10.1016/j.automatica.2009.06.005.
[30] Muske KR, Rawlings JB. Model predictive control with linear models. AIChE J 1993;39(2):262–87. http://dx.doi.org/10.1002/aic.690390208.
[31] Tippett MJ, Tan CK, Bao J. Non-constant prediction-step MPC for processes with multi-scale dynamics. IFAC Proc Vol 2014;47(3):3068–73. http://dx.doi.org/10.3182/20140824-6-ZA-1003.01093.
[32] Mayne DQ, Rawlings JB, Rao CV, Scokaert PO. Constrained model predictive control: Stability and optimality. Automatica 2000;36(6):789–814. http://dx.doi.org/10.1016/S0005-1098(99)00214-9.
[33] Schmid JC. Development of a novel dual fluidized bed gasification system for increased fuel flexibility [Ph.D. thesis], TU Wien; 2014, http://dx.doi.org/10.34726/hss.2014.25397.
[34] Diem R. Design, construction and startup of an advanced 100 KW dual fluidized bed system for thermal gasification [Ph.D. thesis], TU Wien; 2015.
[35] Schmalzl M. Implementierung der MSR-Technik einer 100 kW dual fluid versuchsanlage zur vergasung von festbrennstoffen [Master Thesis], TU Wien; 2014, http://dx.doi.org/10.34726/hss.2014.23536.
[36] Hammerschmid M, Rosenfeld DC, Bartik A, Benedikt F, Fuchs J, Müller S. Methodology for the development of virtual representations within the process development framework of energy plants: From digital model to digital predictive twin-a review. Energies 2023;16(6). http://dx.doi.org/10.3390/en16062641.
[37] Lofberg J. YALMIP : a toolbox for modeling and optimization in MATLAB. In: 2004 IEEE international conference on robotics and automation (IEEE cat. no.04CH37508). 2004, p. 284–9. http://dx.doi.org/10.1109/CACSD.2004.1393890.
[38] The Mathworks Inc. MATLAB Optimization Toolbox. 2022, URL https://www.mathworks.com/products/optimization.html.